Author Manuscript

Author Manuscript

Author Manuscript

Author Manuscript

HHS Public Access

Author manuscript

Biomaterials. Author manuscript; available in PMC 2024 January 01.

Published in final edited form as:

Biomaterials. 2023 January ; 292: 121912. doi:10.1016/j.biomaterials.2022.121912.

Liquid Crystal Elastomer Based Dynamic Device for Urethral Support: Potential Treatment for Stress Urinary Incontinence

Seelay Tasmim[1], **Zuha Yousuf**[2], **Farial S. Rahman**[2], **Emily Seelig**[1], **Abigail Clevenger**[1], **Sabrina VandenHeuvel**[1], **Cedric Ambulo**[3], **Shreya Raghavan**[1], **Philippe E. Zimmern**[4], **Mario I. Romero-Ortega**[2], **Taylor H. Ware**[1,*]

[1]Department of Biomedical Engineering, Texas A&M University, College Station, TX, 77843, USA

[2]Departments of Bioengineering and Biomedical Science, University of Houston, Houston, TX, 77004, USA

[3]Materials and Manufacturing Directorate, Air Force Research Laboratory, Dayton, OH, 45433, USA

[4]Department of Urology, The University of Texas Southwestern, Dallas, TX, 75390, USA

Abstract

Stress urinary incontinence (SUI) is characterized by the involuntary loss of urine due to increased intra-abdominal pressure during coughing, sneezing, or exercising. SUI affects 20-40% of the female population and is exacerbated by aging. Severe SUI is commonly treated with surgical implantation of an autologous or a synthetic sling underneath the urethra for support. These slings, however, are static, and their tension cannot be non-invasively adjusted, if needed, after implantation. This study reports the fabrication of a novel device based on liquid crystal elastomers (LCEs) capable of changing shape in response to temperature increase induced by transcutaneous IR light. The shape change of the LCE-based device was characterized in a scar tissue phantom model. An *in vitro* urinary tract model was designed to study the efficacy of the LCE-based device to support continence and adjust sling tension with IR illumination. Finally, the device was acutely implanted and tested for induced tension changes in female multiparous New Zealand white rabbits. The LCE device achieved 5.6% ± 1.1% actuation when embedded in an agar gel with an elastic modulus of 100 kPa. The corresponding device temperature was 44.9°C ± 0.4°C, and the surrounding agar temperature stayed at 42.1°C ± 0.4°C. Leaking time in the *in vitro* urinary tract model significantly decreased ($p<0.0001$) when an LCE-based cuff was sutured around the model urethra from 5.2min ± 1min to 2min ± 0.5min when the cuff was illuminated with IR light. Normalized leak point force (LPF) increased significantly ($p=0.01$) with the implantation of an LCE-CB cuff around the bladder neck of multiparous rabbits. It decreased

*Corresponding Author. taylor.ware@tamu.edu.

Publisher's Disclaimer: This is a PDF file of an unedited manuscript that has been accepted for publication. As a service to our customers we are providing this early version of the manuscript. The manuscript will undergo copyediting, typesetting, and review of the resulting proof before it is published in its final form. Please note that during the production process errors may be discovered which could affect the content, and all legal disclaimers that apply to the journal pertain.

Declaration of interests

The authors declare that they have no known competing financial interests or personal relationships that could have appeared to influence the work reported in this paper.

Author Manuscript Author Manuscript Author Manuscript Author Manuscript

significantly (p=0.023) when the device was actuated via IR light illumination. These results demonstrate that LCE material could be used to fabricate a dynamic device for treating SUI in women.

Keywords

Liquid Crystal Elastomers; Artificial Muscle; Direct Ink Writing; Stress Urinary Incontinence

1. Introduction

Stress urinary incontinence (SUI) is a condition where increases in the intra-abdominal pressure, such as with coughing or laughing, leads to involuntary urine leakage. This condition is most predominant in women affecting 20-40% of the adult population and 77% of the elderly [1]. This condition can take a significant toll on a patient's quality of life and can be a source of embarrassment and financial burden accounting for an annual economic burden of over $12 billion in the US, where patients pay up to $900 annually [2,3]. The main factors that affect continence are bladder neck position, urethral sphincter closure efficiency, and urethral support. The urethra is supported via the anterior vaginal wall, the levator ani muscle, the endopelvic fascia, and the arcus tendineus fasciae pelvis [4,5]. To maintain continence, the urethral closure pressure exceeds the bladder pressure, via the active constriction of the striated urethral sphincter muscles and the contraction of the peri-luminal urethral longitudinal smooth muscles [4]. In normal conditions, the bladder neck and the urethra are compressed against the hammock-like vaginal supportive layer, which increases urethral pressure by sealing the urethral lumen closed in response to increased bladder pressure [6,7]. Intraabdominal pressure increases with activities like coughing and sneezing. In patients affected by SUI, this increase in abdominal pressure can cause the vaginal wall to move down and pull the urethra open, resulting in involuntary leakage. Urethral sphincter dysfunction, known as intrinsic sphincter deficiency (ISD), and structural failure of the urethral supportive layer, known as urethral hypermobility, are the main mechanisms behind SUI [8–10]. While the etiology of SUI is still unknown, urethral and pelvic floor muscle atrophy with aging, pregnancy, and vaginal birth are contributing factors leading to SUI in women [11].

Patients with a low to moderate level of SUI can benefit from non-surgical intervention to treat their symptoms, such as behavioral therapy and fluid intake optimization [12], hormone therapy [13], pelvic floor muscle training [14], and injecting bulking agents [15]. Patients with more severe SUI, in whom conservative treatment methods failed, require surgical intervention [16]. The gold standard in surgical intervention for SUI treatment is the insertion of synthetic or autologous sling underneath the urethra to provide the needed support. The sling procedure is an invasive method with a highly variable objective cure rate of 57-92%, depending on the patient's age, the severity of SUI, and the duration between the sling implantation and follow-up evaluation [17–19]. According to one study, the objective cure rate after one year of sling implantation among young, middle-aged, and old women was 91%, 81%, and 67%, respectively [19]. The primary function of these slings is to improve continence by supporting the urethra. However, this support and compression

Author Manuscript Author Manuscript Author Manuscript Author Manuscript

can lead to potential complications with voiding since these slings are static and cannot change configuration once implanted. For instance, polypropylene synthetic slings can cause overtightening of the urethra during the healing process, which involves scarring and retraction [20–22]. A tight sling can cause urine retention, leading to chronic urinary tract infections, bladder overactivity, and a lifelong need for intermittent catheterization [23]. A sling placed loosely in an effort to prevent the above complications can lead to residual SUI. This dilemma between a sling that may end up being loose or too tight creates a need for designing a new sling with dynamic properties to correct SUI without a negative impact on the voiding function.

Artificial muscles (i.e., biomedical devices that can change shape reversibly) can assist in treating many health conditions such as prosthetic limbs, artificial heart valves, and artificial sphincters. Fabricating such devices requires certain important considerations: the amplitude and response time of the device, power source, and the device's ability to deform for thousands (or more) cycles. Active devices traditionally have motors and pumps with a battery power source. Such heavily tethered devices have limited use in biomedical applications [24]. Stimuli-responsive materials that change shape (i.e., elongate, contract, and/or twist) when exposed to an appropriate stimulus are promising candidates to replace traditional machines in biomedical devices [25]. For instance, shape memory alloys (SMA) have been proposed for the fabrication of artificial muscles in both tensile [26–28] and hybrid [29,30] configurations. However, SMA-based devices that produce large forces generate limited deformations [31,32]. Stimuli-responsive gels are capable of swelling and deswelling in response to certain stimuli and have been proposed for use as artificial muscle actuators [33,34]. However, while stimuli-responsive gels can achieve significant volumetric changes, they are limited due to their inability to generate large forces and relatively slow response times [35], restricting their use as artificial muscles.

Liquid crystal elastomers (LCEs) are a class of stimuli-responsive soft materials that can be programmed to change shape in a controlled and reversible manner without the need for tethered power sources [36]. These materials have two main phases, the low-temperature nematic phase (phase of molecular order) and the high-temperature isotropic phase (phase of molecular disorder). If the nematic phase of the LCE precursor is oriented in a specific direction and then crosslinked, the shape change of the material can be programmed [36–38]. LCE-based devices have been shown to achieve large reversible actuation strains and produce moderate work outputs [39,40]. While the large reversible actuation strain, work output, and desirable mechanical properties of LCEs have been widely recognized [41–43], two main limitations prevent LCE utilization in biomedical applications. First, the temperature needed for shape change is usually too high to be acceptable in a physiological environment. Second, it usually requires direct application of heat, which is not realistic in many biomedical applications. Previously we described an LCE synthesis route where LCEs synthesized via thiol-ene click reaction, yielding thiol-terminated liquid crystalline oligomers, achieve considerable shape change (20%-30%) in response to physiologically relevant temperatures [43–45]. This approach was built on a variety of similar approaches using thiol-ene chemistry to control the network architecture and transition temperature of LCEs [46–49]. We utilize these LCEs with actuation temperatures in the range of 35°C - 45°C, which can be safe in the physiological environment [50]. The ability to design

Author Manuscript Author Manuscript Author Manuscript Author Manuscript

LCE composite systems that can absorb light or produce electrical activity allows for facial control of these devices [51–53]. For example, incorporating infrared (IR)-absorbing carbon black (CB) particles allows the shape change of the LCE material to be triggered with IR light illumination where incident light locally heats the material. IR light can penetrate through tissue and is utilized in many thermal therapies, such as skin rejuvenation [54].

By utilizing the reversible actuation of LCEs, we fabricate an artificial muscle that changes shape and functions like a urethral sphincter. Here, we prototyped a 3D printed LCE-CB composite device in a sling and cuff configuration that can change shape reversibly in response to a safe range of IR light intensity. This device will normally support the urethra (sling) or surround it (sphincter) to restore continence. Once illuminated with IR light, the LCE-CB sling changes shape, reducing urethral support, and allowing for unimpeded voiding. In this study, we focused on evaluating the LCE-CB cuff device. We tested the shape change and temperature response of the LCE-CB samples in physiological conditions and in response to a physiologically safe intensity of IR light. The efficacy of an LCE-CB cuff to improve continence and then allow for unimpeded voiding on IR illumination was first assessed *in vitro* in a custom-made *in vitro* urinary tract model and acutely *in vivo* in anesthetized multiparous rabbits.

2. Materials and Methods:

2.1. Material/Ink Synthesis

The LCE was fabricated using liquid crystal monomer 1,4-bis-[4-(6-acryloyloxyhexyloxy) benzoyloxy]-2-methylbenzene (RM82) (Wilshire Technologies), a thiol chain extender 2,2'-(ethylenedioxy) diethanethiol (EDDT) (Sigma-Aldrich), vinyl crosslinker 1,3,5-Triallyl-1,3,5-triazine-2,4,6(1H,3H,5H)-trione (TATATO) (Sigma-Aldrich), photoinitiators, Irgacure 1-369 and Irgacure I-819 (Sigma-Aldrich), radical inhibitor butylated hydroxytoluene (BHT) (Sigma-Aldrich), and base-catalyst Triethylamine (TEA) (Sigma-Aldrich). IR absorbing carbon black (CB) particles, PDMS (Sylgard 184), agar, and sulforhodamine B sodium salt dye were purchased from Sigma-Aldrich.

Thiol-terminated liquid crystal ink with embedded carbon black particles was synthesized via the Michael Addition of acrylate mesogens and thiol chain extenders at a molar ratio of 0.8(RM82):1(EDDT):0.2(TATATO) heated to 80°C and mixed. A 1 wt% of the acrylate amount BHT, 3.5 wt% of photoinitiator with a ratio of 0.25(I-819):0.75(I-369), 1 wt% of TEA, and variable concentrations of CB (0 wt%, 0.2 wt%, or 0.4 wt%) were mixed with the solution. After thoroughly mixing the chemicals, the ink was transferred to a 3D printing syringe and allowed to oligomerize for 3 hours at 65°C and then at room temperature for 12 hours.

2.2. Direct Ink Writing (DIW)

The 3D printing syringe with the LCE ink was loaded onto a KR-2 extruder print head, an attachment to the System 30M 3D printer from Hyrel3D (Norcross, GA, USA). The ink was printed at 38°C with a uniaxial print path. The filaments were aligned along the rectangle's width using a 24G stainless steel dispensing needle with an inner diameter of

Author Manuscript Author Manuscript Author Manuscript Author Manuscript

310μm. A print speed of 3 mm/s was used. A 365nm UV curing LED provided with the KR-2 printhead was used for immediate photocrosslinking of the LCE-CB ink at 1.5W/cm^2 intensity during the entire 3D printing process. Further crosslinking was carried out after 3D printing by continuous UV illumination of the printed structure from an OmniCure LX400 LED UV curing system (Excelitas Technologies, Waltham, MA, USA). The UV light was kept at 13cm distance from the samples, which resulted in UV intensity of 2W/cm^2 at the 3D printed structure surface. Samples were illuminated with UV light for 20 minutes on each side. Samples with increased CB concentration required a longer UV curing time of 30 minutes for each side.

2.3. Material Characterization

2.3.1. Differential Scanning Calorimetry—To analyze thermal properties, such as the nematic to isotropic transition temperature (T_{NI}) of the ink, differential scanning calorimetry (DSC) analysis was performed using TA Instruments Q20 (New Castle, DE, USA). Approximately 10mg LC ink with variable CB concentration (0wt%, 2wt%, and 0.4 wt%) was loaded into a DSC pan. Samples at ambient temperature were heated to 100°C, cooled down to room temperature, and then reheated to 100°C at 10°C/min rate. Heat flow data collected from the second heating cycle was then used to determine T_{NI} for neat LC ink and LC-CB ink with 0.2 wt% and 0.4 wt% CB. Each ink composition was synthesized in three batches, and three samples were tested from each batch. (n=9).

2.3.2. Rheological Analysis—The rheological properties of the LC ink with varying CB concentrations were studied using a Discovery HR-2 rheometer TA Instrument (New Castle, DE, USA). A 25 mm parallel plate geometry with a gap of 300μm was used with logarithmic shear rate sweep from 0.01 s^{-1} – 100 s^{-1}. All inks were kept at the printing temperature of 38°C during testing. Each ink composition was synthesized in three batches, and three samples were tested from each batch. (n=9).

2.3.3. Dynamic Mechanical Analysis (DMA)—DMA was performed to determine the storage modulus and tan delta associated with a neat LCE using TA instrument RSA-G2 (New Castle, DE, USA). 1mm thick polydomain LCE strips were prepared by injecting the LCE precursor mixture into a glass capillary cell with a 1mm gap. The material was allowed to oligomerize in the oven at 65°C for three hours, then at room temperature for 12 hours. The oligomer within the glass capillary cell was then photocrosslinked using an OmniCure LX400 LED UV spot curing system for 10 minutes on each side. The polydomain LCE sample was removed from the glass cell and cut into 3mm by 15 mm strips for testing. Samples were loaded onto the DMA with a loading gap of 10 mm and tested at 0.3% strain at 37°C from 0.1Hz – 10Hz. Samples were fabricated from three batches, and three samples from each batch were tested (n=9).

2.3.4. In Vitro Cytotoxicity Testing—Primary human dermal fibroblasts (hDFAs) were a gift from the Zhao lab in the Biomedical Engineering Department at Texas A&M University. Cell culture reagents used in this study, including nutrient medium and a live/dead cell imaging kit, were purchased from Thermo Fisher Scientific (Waltham, MA) unless otherwise specified. Cytotoxicity assays were carried out in accordance with the ISO 10993:

Author Manuscript Author Manuscript Author Manuscript Author Manuscript

"Biological evaluation of medical devices", Part 5: "Test for invitro cytotoxicity". Extracts were prepared in accordance with ISO 10993, Part 12: "Sample preparation and reference materials".

2.3.4.1. Extract Preparation: All samples were disinfected prior to use by submerging in 70% ethanol for two hours, washing with sterile PBS three times, and then UV irradiating for one hour on each side using a UV lamp with a wavelength of 254nm (Analytik Jena, Upland, CA, USA). Extracts were prepared by incubating both LCE-CB samples and Tygon F-4040-A PVC tube (positive control) in complete media with 3 cm^2 surface area for every 1mL of media (according to ISO 10993-5 and ISO 10993-12). Media with samples were placed in New Brunswick's model I24 benchtop incubating shaker (Eppendorf, Hauppauge, NY) at 37°C and 200 rpm for 24 hours.

2.3.4.2. Cell Culture and Cytotoxicity analysis: Primary Human dermal fibroblasts (hDFAs) were cultured in Dulbecco's Modified Eagle Medium supplemented with Nutrient Mixture F-12 (Thermo Fisher Scientific), 1X antibiotics and 20% fetal bovine serum. hDFAs were cultured on tissue culture dishes until 80% confluency. To maximize seeding of hDFAs on coverglass chamber slides, Collagen I (200 μg/mL) was used to coat the chambers. Collagen-coated coverglass was stored at 4°C until use. hDFAs were seeded on coverglass at 7,500 cells/mL and incubated overnight to allow for attachment. All cultures were incubated at 37°C with 5% CO_2 and 95% humidity. Following cell adherence overnight, media was replaced with 1 ml of fresh growth media (negative control), or extract media from LCE-CB (test), or Tygon (positive control), respectively. Cells were imaged using phase contrast immediately following media replacement and after 24 and 48 hours. A calcein-AM/ethidium homodimer-based live/dead assay was performed at 48 hours following the manufacturer's protocol (Thermo Fisher Scientific). Fluorescent imaging consisted of green fluorescence in live cells (calcein-AM) and red fluorescence in dead cells (ethidium honmo-dimer). Fluorescence was observed using a Leica DMi8 Microscope (Wetzlar, Germany), with five independent, non-overlapping regions for analysis. NIH ImageJ was utilized to perform fluorometry. Live and dead cells were identified by the presence of green or red fluorescence, respectively, and quantified manually. Analysis was performed to determine the number of live cells versus the total cell number to determine the percentage of live cells.

2.4. Actuation Characterization

2.4.1. Thermal Actuation—Shape change of the LCE samples in response to ambient temperature change was analyzed using image analysis software (ImageJ). 5mm x 6mm uniaxially aligned LCE samples with varying CB concentrations (0 wt%, 0.2 wt%, and 0.4 wt%) were immersed in silicon oil, heated above 50°C on a hot plate, and equilibrated for 3 minutes. A Canon DSLR camera (EOS Rebel T7i) fitted with a 100 mm macro lens was used to capture optical images of the sample on cooling from 50°C to 35°C with 1°C increment. Change in the sample width as a function of temperature was determined using the image analysis software. Actuation strain (denoted as % width contraction) was calculated using the following equation:

Author Manuscript Author Manuscript Author Manuscript Author Manuscript

$$\% \ Width \ contraction = \frac{(L_o - L_f)}{L_o} * 100\%$$

Where L_o represents the initial length before heating and L_f represents the final length after heating along the print path. As the IR light intensity may vary across the sample, dimensional changes were measured at the top, middle, and bottom of each experimental replicate. Samples for each composition were fabricated from three batches, and three samples from each batch were tested (n=9 for each composition).

2.4.2. NIR Actuation—To analyze shape change with IR illumination, LCE samples with 0 wt%, 0.2 wt%, and 0.4 wt% were embedded in a soft agar gel with a 0.5% agar concentration and placed in a water bath at 37°C. To keep the water bath at 37°C, the TC200 temperature controller (Thorlabs, Newton, NJ, USA) was used with the HT19R metal ceramic heater and TH10K thermistor (Thorlabs, Newton, NJ, USA). A 735nm IR LED with light intensity adjustment capabilities, CBM-120-FR (Luminus Devices Inc., Sunnyvale, CA, USA), was used to illuminate the sample from the bottom for two minutes. The IR LED was connected to a laboratory-grade switching mode DC power supply with voltage and current adjustment capabilities (Extech, Nashua, NH, USA). The IR intensity was controlled by adjusting the voltage and current provided to the LED by the power supply. Samples were photographed before and after IR illumination at intensities in the range of 200mW/cm^2 - 800mW/cm^2 with increments of 50mW/cm^2. The voltage and current setting for each desired IR light intensity at a specific distance were measured using the PM160 power meter (Thorlabs, Newton, NJ, USA). A Fisherbrand 15-078-186 Type K thermocouple was used to measure the temperature of the sample surface and agar at 2mm from the sample by placing the thermocouple lead into the agar gel surrounding the sample. Sample surface temperature was collected at three different points on the sample for each time point. The equation used for calculating actuation strain with thermal actuation was also used for IR actuation. Samples for each composition were fabricated from three batches, and three samples from each batch were tested (n=9 for each composition).

2.4.3. NIR Actuation in Scar Tissue-Like Environment—LCE with 0.4wt% CB was used to analyze shape change in scar-tissue-like environment by embedding LCE-CB samples in agar gels with varying agar concentrations (0.5% agar concentration, 1% agar concentration, and 1.25% agar concentration). After embedding samples in agar gels, they were placed in a water bath at 37°C and illuminated with 500mW/cm^2 for two minutes. Shape change was photographed every 30 seconds to calculate actuation strain. Temperatures at the sample surface and agar in the 2mm vicinity were measured every 30 seconds. Samples were fabricated from three batches, and each batch was tested three times (n=9).

2.4.4. Actuation Curve—The actuation curve of the LCE-CB sample with 0.4 wt% CB embedded in 1% agar gel was determined by analyzing the shape change of the sample with IR illumination for 90 seconds and IR off for 60 seconds. Samples were photographed every

Author Manuscript Author Manuscript Author Manuscript Author Manuscript

15 seconds, and their actuation strain was calculated in both the IR on and IR off conditions. One sample was tested over three cycles of IR on and IR off.

2.4.5. Cyclic Actuation—To analyze the shape change and temperature response, we tested samples with 0.4 wt% CB embedded in 1% agar gel over 100 cycles of IR on and IR off conditions. Samples were photographed before, immediately after, and 60 seconds after illumination with 500mW/cm^2 IR light for two minutes. The temperature at the sample surface and agar in the 2mm vicinity was measured before, immediately after, and 60 seconds after two minutes of IR illumination. Actuation strain was calculated by analyzing the shape change images with the image analysis software.

2.5. LCE-CB Cuff *In Vitro* Analysis

2.5.1. *In vitro* Urinary Bladder-Urethra Model Preparation—The *in vitro* model was built utilizing a synthetic bladder (SynDaver, Tampa, FL, USA) and a two-part artificial urethra made with a soft PDMS tube and a stiff PDMS plug. To prepare the custom-made urethra, a soft PDMS hollow tube with an inner diameter of 8 mm and a wall thickness of 1 mm and a cylindrical PDMS plug with a 7.5 mm diameter were prepared with molds. A curing agent to base ratio of (1:45) and (1:10) of PDMS was used to fabricate the soft tube and hard plug, respectively (Supporting Fig. S1A and B). After pouring the PDMS in their respective molds, they were cured in an oven at 70°C for at least 12 hours. To ensure water flow through the soft PDMS tube from the bladder, one end of the urethral plug was tapered to reduce its diameter to 0.5 mm (Supporting Fig. S1A). The narrow end of the urethral plug was then glued onto the inside of the urethral opening in the SynDaver bladder model (Supporting Fig. S1B). The stiff PDMS plug was inserted inside the soft PDMS tube, and the PDMS urethral tube was glued around the urethral opening of the SynDaver model (Supporting Fig. S1C).

2.5.2. LCE-CB Cuff Preparation—An LCE-CB cuff was designed to function as an artificial sphincter around the *in vitro* urethra model and was sutured around the model urethra. To allow for the LCE-CB cuff to prevent the extension of the soft PDMS tube due to increased back pressure with bladder filling, the cuff was designed to fit snugly around the model urethra. To achieve that, the cuff circumference was designed to be the same length as the circumference of the model urethra. For our model urethra, an LCE-CB rectangular sample with 0.4 wt% CB was printed with a 10mm width and 29 mm length (Supporting Fig. S2A and B). The rectangle was wrapped around the model urethra as a cuff, and the two ends were sutured together (Supporting Fig. S2C).

2.5.3. *In Vitro* Urinary Model—To simulate physiological conditions, a slab of agar gel with 1% agar concentration was molded to fit around the modeled urethra mimicking scar tissue surrounding the implanted cuff (Supporting Fig. S3A and B). The *in vitro* model was then placed on an angled stage where the bladder was at an angle of ~60°, and the urethra was at an angle of ~23° (Supporting Fig. S3C).

2.5.4. Leakage Volume Measurement with and Without LCE-CB Cuff—The *in vitro* urinary tract model was used to measure the ability of an LCE-CB cuff to prevent

Author Manuscript Author Manuscript Author Manuscript Author Manuscript

leakage and allow for voiding on IR illumination. We first measured the voiding time of the urethra model without the LCE-CB cuff. We injected 20 mL of water into the artificial bladder through one of the ureters. The water was heated to ~50°C before injecting in the model, so due to the device being placed at room temperature (~28°C), the final temperature of the water inside the bladder and flowing through the urethra was around 37°C. The water was dyed with sulforhodamine B sodium salt dye for better visualization. A petri dish was used to collect voided water for voided volume measurement, and time to complete voiding was recorded. This experiment was repeated after an LCE-CB cuff was sutured around the model urethra. The bladder was again filled with 20mL of water, and the voiding time and voided volume were recorded. Finally, to measure the voiding time for the *in vitro* model with the LCE-CB cuff and IR on condition, the LCE-CB cuff was illuminated with IR light of 500 mW/cm^2 – 600mW/cm^2 intensity. The experiment was performed in the same manner as the previous two conditions. Three different LCE-CB cuffs were used, and voiding time with IR on and IR off conditions was measured three times with each cuff (n=9).

Finally, one LCE-CB cuff from the previous experiment was used to analyze the behavior of the LCE-CB cuff over multiple cycles of testing. Each cycle consisted of measuring voiding time and voided volume with the LCE-CB cuff and IR off condition, followed by IR on condition. Measurements were made over 15 cycles, and a 5-minute break was allowed between each cycle.

2.6. LCE-CB Cuff *In Vivo* Analysis

2.6.1. Animals—Three adult female multiparous New Zealand white rabbits (14-18 months, 4-5 kg, Charles River Laboratories International, Inc) were used for the *in vivo* analysis of the LCE-CB cuff. Animals were group-housed in a temperature (22°C ± 1°C) and humidity (30 – 70%) controlled room on a 12:12 hour light/dark cycle with ad libitum access to water and fed a complete diet for adult rabbits. All experimental procedures were performed at an AAALAC accredited vivarium, and animal care followed the standards established by the National Research Council Guide for the Care and Use of Laboratory Animals. Animal handling and surgical protocol were approved by the University of Houston Institutional Animal Care and Use Committee protocol number PROTO202000049.

Anesthesia was induced using 35 mg/kg ketamine and 5 mg/kg xylazine and maintained using propofol at a constant infusion rate of 0.6 mg/kg/min. When an adequate depth of anestesia was attained (loss of corneal reflex) the rabbits were placed in supine position and a 3-4 cm incision was made upward from the pubic crest at the midline under sterile conditions through facia to reveal abdominal muscles, which were incised at the midline. The adipose tissue was then removed to expose the bladder and blunt dissect the bladder neck from the uterine wall (Fig. 7). A 21G blunt butterfly needle was inserted at the bladder apex, and sutured in place via a purse-string suture using 6-0 non-absorbable suture. Following apical implantation, the abdominal muscles and skin were sutured close to maintain abdominal pressure. Baseline cystometry and leak point force (LPF) data were collected using the urodynamic system described in the next section. To analyze the performance of the LCE-CB as a urethral sphincter, rabbit bladder neck circumference

Author Manuscript Author Manuscript Author Manuscript Author Manuscript

was measured *in situ*, and a rectangular piece of LCE-CB was cut to the size of the rabbit bladder neck circumference. To expose the bladder neck, the incision above this area was reopened and the LCE-CB was sutured around the bladder neck as a cuff using 6-0 non-absorbable sutures (Oasis Nylon Monofilament Suture) (Fig. 7C). The incision was closed after completing device implantation. Under constant anesthesia and constant bladder filling, five replicate measurements of leak point force (see below) were obtained in three rabbits. The total procedure took 4-6 hours and AALAS certified animal health technicians provided appropriate animal physiological monitoring during the surgical procedure. At the end of the study, the animals were euthanized by overdosing with pentobarbital (120mg/kg, ip).

2.6.2. Cystometry—The bladder catheter was connected to a custom-built urodynamic system consisting of the following: 1) an air-filled calibration syringe connected to a pressure gauge, 2) a saline-filled syringe for flushing the tubing, and 3) a pressure transducer (MLT0699 Disposable BP Transducer) for measuring intravesical pressure. The urodynamic set-up was connected to a syringe pump (NE-1000 Programmable Single Syringe Pump, New Era Pump Systems, Inc) for bladder filling (Fig. 7A) using warm 0.9% saline solution. The pressure transducer was connected to a bridge amplifier and Powerlab (ADInstruments, Colorado Springs, CO), and Lab Chart software (ADInstruments, Colorado Springs, CO) to record intravesical pressure during cystometry [55] (Fig. 7A).

The cystometry was performed to determine maximum bladder capacity, defined as the bladder volume prior to urine leakage [56] (Fig. S4). The cystometry set-up was zeroed and flushed using saline. The system was connected to the implanted butterfly needle, and a two-point calibration from 0 mmHg to 40 mmHg was done. The syringe pump was used to fill the bladder with 0.9% saline solution (~37°C) at a rate of 2mL/min. The process for determining bladder capacity for each rabbit is explained in the supplementary information.

2.6.3. Leak Point Force (LPF) Analysis—The bladder was filled to half capacity with warm saline using the syringe pump at a 2 mL/min flow rate. Filling the bladder to half capacity ensured that urine leakage events resulted from the increased abdominal force and not the bladder being at threshold volume [57]. Leak point force (LPF) in this study was defined as the maximum force exerted on the rabbit abdomen that caused leakage (Fig. 7D). A load cell (iLoad mini, Loadstar Sensors, Fremont, CA) mounted on an application pad of polystyrene thermocol was used to apply gradual force on the abdomen on top of the bladder dome until a leakage event was observed (Fig. 7D). Force applied was recorded using LoadVUE software connected to the load cell. Prior to use, the load cell was tared after placing it on the approximate area of the rabbit bladder (3-4 cm above the pubic symphysis). Applied force on the rabbit abdomen was discontinued immediately after a leakage event was observed. Simultaneously, LPF value on the LoadVUE software was recorded. LPF was measured with five repetitions in each rabbit with at least 1-minute rest time. The experiment was performed under four different conditions: 1) before implanting LCE-CB cuff around the bladder neck (baseline), 2) after device implantation (Implant), 2) after the device was illuminated with 60 seconds of IR light with 500-600mW/cm^2 (Implant + IR ON), and 4) with no IR light illumination (Implant + IR OFF). Prior to starting LPF

Author Manuscript Author Manuscript Author Manuscript Author Manuscript

testing at each condition, the bladder was emptied manually using a syringe then filled to half capacity via the implanted butterfly needle.

2.7. Statistical Analysis

Data are presented as the mean ± standard deviation for all experiments with experimental replicates and analyzed with GraphPad Prism 9.4.0. Statistical comparison of the actuation strain and temperature increase of neat LCE samples, LCE-CB samples with 0.2 wt% CB, and LCE-CB samples with 0.4 wt% CB was carried out via the one-way ANOVA test. Comparison within the three groups was carried out using the Tukey Kramer test. Statistical comparison of the average voiding time with IR on and IR off conditions was determined using paired student's t-test. Pairwise comparisons between the three groups (Baseline vs. Implant; Implant vs. Implant + IR ON; Implant vs. Implant + IR OFF) were carried out using the paired t-test. A significance level of 0.05 was used, and $p<0.05$ was used to consider the difference in the averages statistically significant. Power analysis calculations were carried out considering a minimum effect size of 3, with power of 80%, and a significance level of less than 5% to determine the sample size at which statistically significant difference in the in vivo study would be demonstrated.

3. Results

3.1. LCE-CB Sample Fabrication:

To fabricate an artificial muscle that could be used to treat SUI, three main requirements need to be met. First, the material should be processable in such a way that enables programming a specific shape change response. Shape change in LCEs is controlled via preprogramming the desired molecular orientation in the structure. Second, since the device must be triggered to change shape within the body, the material must undergo actuation at temperatures tolerated by human tissue. Third, the device must actuate reversibly for many cycles even when encapsulated in tissue. Device implantations in the body are always followed by the healing process, which includes scar tissue generation around the implant [58,59]. Thus, the device must produce sufficient force to change shape even in a scar-tissue-like environment. We chose to use direct-ink-write printing of LCE-CB composites to achieve these goals.

We fabricated the LCE-CB device via a two-step thiol-ene reaction scheme between a liquid crystal mesogen with acrylate end groups, a dithiol chain extender, and a trivinyl crosslinker (Fig. 1A) [43]. First, liquid crystalline ink was synthesized via the Michael Addition of the dithiol with the liquid crystalline diacrylate. In this reaction, the LC mesogen (RM82) with acrylate end groups reacted with thiol (EDDT), generating thiol-terminated oligomers. To enable heating of the device within the body, CB particles were added to the ink to enable the material to become responsive to IR light. The liquid crystalline oligomer mixture with CB has the appropriate rheological properties for direct-ink-write printing.

The device must elongate/expand with IR illumination for better voiding condition and contract back to its original shape to provide the necessary support for continence. During 3D printing, the thiol-terminated LC polymerized ink is aligned via DIW where the shear

Author Manuscript Author Manuscript Author Manuscript Author Manuscript

forces align the polymer chains in the direction of the print path as it is exiting the nozzle [60–62] (Fig. 1B). Prior work in printed LCEs have shown that the shear forces while 3D printing are sufficient to introduce an orientational order within the LC polymer network. For instance, Ambulo et al. show the alignment of extruded LC inks in both neat [60] and liquid metal composite [53] LCEs using polarized optical micrographs, while Ren et al. demonstrate this using X-ray diffraction images[63]. This alignment is locked in by the thiol-ene radical reaction between the oligomers and the triallyl crosslinker. When IR light is illuminated, the rectangular device contracts along its short axis, which leads to its overall elongation (Fig. 1C). The photoresponsive device was tested in an artificial urethral model, and IR was illuminated to cause device elongation leading to reduced urethral support (Fig. 1D).

3.2. LCE-CB Material Characterization

Thermal analysis of the LCE ink was carried out via differential scanning calorimetry (DSC) test to determine the temperature at which the ink transitions from the ordered nematic phase to the isotropic phase (T_{NI}). DSC curve showed an endothermic peak at 42.5°C ± 1°C, indicating that this ink has a relatively low T_{NI} (Fig. 2A). The incorporation of 0.2wt% and 0.4wt% CB particles in the LC did not substantially affect the transition temperature of the ink. The composite inks exhibit shear-thinning akin to neat LC inks. The viscosity of the ink increases slightly at low shear rates with increasing the CB concentration from 0.2 wt% to 0.4 wt% (Fig 2B). After crosslinking, the shape change of the rectangular LCE samples with and without CB was studied by plotting the width contraction of the sample with increasing temperature (Figure 2C).

To analyze the use of LCE-CB material as an artificial muscle device, we evaluated the cytotoxic effect of this material in accordance with the ISO protocol 10993-5 primary human dermal fibroblast (hDFAs). For this, hDFAs were maintained with growth media (negative control), LCE-CB extract media, or Tygon extract media (positive control) over 2 days and their viability was monitored. Phase images were taken at 0 hours, 24 hours, and 48 hours to track cell growth (Fig 2E). Rounded sparser cells were observed in the media conditions that contained Tygon extracts, indicating cell death. In contrast, elongated adherent cells were observed in the control or LCE-CB extract conditions. While control and LCE-CB extract exposed cells continued to remain healthy at both 24 and 48 hour time points, Tygon extract exposed cells died as early as 24 hours after exposure. In order to quantify cell viability upon extract exposure, we utilized a live/dead fluorescence assay kit, that stained live cells green and dead cells red. Cells were stained with the live/dead assay after 48 hours of exposure to 100% extracts (negative control, positive control, and LCE-CB) (Fig. 2F). The threshold for in vitro cytotoxicity is defined as normalized viability of more than 70% after exposure to extract media. After 48 hours in 100% LCE-CB extract media, hDFAs exhibited cell viability of 91.9% ± 0.8% (mean ± SEM, n=3) (Fig. 2F), which was similar to cell viability for negative control of 99.0% ± 3.5% (mean ± SEM, n=3). Cells exposed to positive control (Tygon extract), however, exhibited a significantly lower normalized viability of 45.1% ± 4.1% (mean ± SEM, n=3, $p<0.0001$). These values are well above the 70% normalized viability threshold set by the ISO standards. As such, these results suggest that LCE-CB material is noncytotoxic to hDFAs.

Author Manuscript Author Manuscript Author Manuscript Author Manuscript

3.3. LCE-CB Sample Shape Change

To understand the shape change response of LCE-CB samples, we prepared LCE-CB composites with varying CB concentrations and irradiated them with varying IR light intensities. Samples were embedded in a soft agar gel (34kPa Modulus), placed in a water bath at 37°C, and illuminated with varying IR light intensities for two minutes (Fig. 3A). Our results show that LCE-CB samples with 0.4wt% CB and 0.2wt% CB could achieve significantly higher temperature increase in response to IR illumination compared to neat LCE samples ($p>0.001$ for each at 500mW/cm^2) but did not significantly differ with 0.2 to 0.4 wt% CB ($p=0.6$ with 500mW/cm^2). As a result, samples with 0.4 wt% CB and 0.2 wt% CB could achieve significantly more actuation strain with IR illumination compared to neat LCE samples ($p<0.001$ with 500mW/cm^2). LCE-CB samples with 0.4 wt% CB achieved 5.7% ± 0.8% actuation strain in response to 500mW/cm^2 IR light intensity (Fig. 3B). At this intensity, the temperature of the sample with 0.4 wt% CB increased to 44.8°C ± 1°C while the temperature of the surrounding agar increased to 41.2°C ± 1.8°C from the 37°C bath temperature (Fig. 3C).

Another requirement for the LCE-CB samples is to change shape even in a stiff, scar-tissue-like environment. Our results show that when illuminated with 500mW/cm^2 IR light, an LCE-CB sample with 0.4 wt% CB can achieve 5.6% ± 1.1% actuation strain in a stiffer gel with 1% agar concentration that has an elastic modulus of around 100kPa [64] (Fig. 4A). In this condition, the temperature of the sample with 0.4 wt% CB was 44.9°C ± 0.4°C, and temperature of the agar surrounding the sample was at 42.1°C ± 0.4°C (Fig. 4B).

It was important that these samples could achieve shape change in a timely fashion over numerous cycles when in a scar tissue-like environment. We first studied the actuation curve of the LCE-CB sample with IR light on for 90 seconds, then off for 60 seconds. Most of the actuation strain can be achieved within the first 30 seconds, and 30 seconds after removing IR light, the sample has mostly returned to its original shape (Fig. 5A). Cyclic actuation of the LCE-CB sample showed that the LCE-CB samples exhibit a relatively stable actuation and temperature response over 100 cycles (Fig. 5B & C).

3.4. LCE-CB Device Analysis *In Vitro*

The device was evaluated for its ability to cause continence and allow for voiding in an *in vitro* urethra model. Due to limitations with designing *in vitro* urinary tract models and animal models feasible for testing a sling device that requires IR illumination through the vaginal canal, an artificial sphincter or a cuff model was evaluated. The cuff was intended to prevent leakage during a high stress or cough condition by limiting flow through the modeled urethra. The LCE-CB cuff could get wider with IR illumination due to LCE material shape change, allowing for better voiding conditions. The *in vitro* model was placed on an angled stage, and a slab of 1% agar gel was used to mimic tissue surrounding the urethra (Fig. 6A). The time for the *in vitro* urinary tract model to void ~20 mL of water was recorded when testing with no LCE-CB cuff around the urethra and with LCE-CB cuff around the urethra with IR light off and on condition (Fig. 6B). The *in vitro* model voided around 19 mL of volume in 0.9min ± 0.1min (Fig. 6C). However, when the LCE-CB cuff was sutured around the urethra, it restricted bladder voiding. As a result, the model voided

Author Manuscript Author Manuscript Author Manuscript Author Manuscript

19 mL of volume in 5.2min ± 1min in this condition, mimicking continence. Finally, when the LCE-CB cuff was illuminated with IR light with an intensity in the range of 500-600 mW/cm^2, the 19mL of volume was voided in 2min ± 0.5min, which was significantly lower than with the IR light off condition (p=0.0397). Video 1 in supplementary information illustrates the initial 15 seconds of voiding in the *in vitro* model without cuff, with cuff IR on, and with cuff IR off conditions.

To show that the LCE-CB cuff can perform with similar behavior in causing continence and allowing for voiding over multiple cycles, an LCE-CB cuff is tested over 15 runs of bladder emptying with IR light off and IR light on back-to-back. The *in vitro* model exhibited a repeatable behavior of bladder emptying with IR off and on conditions over 15 runs (Fig. 6D).

3.5. LCE-CB Device Analysis *In Vivo*

Finally, the LCE-CB device was evaluated in mature, multiparous white New Zealand rabbits. The bladder was filled to half capacity via a syringe pump connected to the bladder using a butterfly needle catheter (Fig. 7A). Intravesical pressure was monitored during bladder filling and baseline cystometry procedures. The LCE-CB device was implanted as a cuff or sphincter around the bladder neck (Fig. 7B & C). The LCE-CB cuff's ability to cause continence and allow for unimpeded voiding with IR illumination was evaluated acutely during manual leak point testing cycles. The cuff was intended to prevent leakage during a high stress or cough condition by limiting urine flow through the bladder neck. Force was gently exerted on the abdomen on top of the bladder dome to cause leakage. This force was defined as the leak point force (LPF) and was measured before implanting the LCE-CB cuff (Baseline), after implanting the LCE-CB cuff (Implant), during illumination of the LCE-CB cuff (Implant + IR ON), and without IR illumination (Implant + IR OFF). The last study group was aimed to evaluate the ability of the LCE-CB cuff to return to its original shape and cause continence. Figure 7E showed a plot of the average normalized LPF values where LPF values in each of the four study groups were divided by the baseline LPF value in each experiment. The average normalized LPF after device implantation was 1.34 ± 0.07, which is significantly higher than that at baseline (p=0.01). Once the device was illuminated with IR light (Implant + IR ON), the average normalized LPF lowered to 0.90 ± 0.07, significantly lower than normalized LPF after device implantation (p=0.023). Finally, after removing the IR light (Implant + IR OFF), the average normalized LPF was 1.34 ± 0.12. Average normalized LPF in the Implant + IR OFF groups had no significant difference compared to the Implant group (p=0.9), indicating that the device returned to its original level of support after the removal of IR light. A plot of the average LPF values for each rabbit is presented in the supplementary information (Fig. S5).

Discussion

In this work, we reported a dynamic device for the treatment of SUI that can, unlike current slings, modulate urethral support postoperatively. Midurethral sling (MUS) placement surgeries are considered the standard-of-care in treating severe SUI in women. These surgeries, however, are associated with complications such as postoperative voiding

Author Manuscript Author Manuscript Author Manuscript Author Manuscript

dysfunction, which can potentially require surgical revisions or sling removal [23]. Urinary retention has been reported in up to 40% of the female population that has undergone MUS placement surgery [21,59,65–68]. While loose slings do not cause sufficient continence, tightening the sling can lead to further complications, leading to potentially unsatisfied patients in either case. Readjustable mid-urethral slings have gained popularity as they are a reasonable alternative for treating or preventing urinary retention [69]. One such sling is the Remeex system (Neomedic International, Terrassa, Spain), which allows postoperative sling tension adjustment through secondary surgery [70]. Devices capable of reversible shape change in the body could modulate and provide urethral tension after implantation without the need for other implantable components.

Stimuli-responsive materials like LCEs can achieve reversible shape change in response to external stimuli and present an interesting potential use for artificial muscles. We hypothesize that when used for fabricating midurethral slings, such materials will have the ability to release some urethral tension on demand leading to better voiding conditions. We first characterized the LCE to ensure that this material could achieve shape change in physiologically relevant conditions. Our results show that the LCE formulation is responsive to temperatures in the range of 37°C – 45°C, which is considered physiologically safe [50]. Moritz and Henriques [50,71] studied the time-temperature relationship for creating second- and third-degree burns using hot water applicators in human and pig skin. Their studies have shown that heating human skin to a temperature of 44°C for up to four hours resulted only in mild hyperthermia in two subjects [50,72]. These studies were later confirmed by Stoll and Greene [73] using more precise thermometry that showed that the minimum pain threshold, which is a more conservative threshold as pain sensation is significantly more sensitive than actual thermal injury[50,73], for human skin is at 43.2°C. They also showed that less serious or no injury was observed with temperatures of up to 44°C for over 100 minutes [50,73]. Roizin-Towel and Pirro observed very little cytotoxicity when heating Chinese hamster ovaries and human cells at 42°C and 43°C for up to 1 hour [74]. Other studies have shown that the critical temperature under which thermotolerance (acquired thermal resistance) can be achieved, also known as the Arrhenius plot breakpoint, lies at around 43.5°C for human cells [50,75–77]. As such, device temperatures below 45°C experienced for less than 5 minutes could be considered physiologically safe.

IR-absorbing CB particles incorporated into the LCE material induced temperature increase in the sling via photothermal effect with IR light illumination without direct application of heat. While increasing CB concentration can enhance photothermal properties, too much CB also increases LCE ink viscosity, making it difficult to 3D print. In our experiments, 0.4 wt% CB concentration is selected as the optimal concentration to ensure 3D printability while also enhancing IR light responsiveness. We envision this device to be implanted as a sling model underneath the urethra. The device can be activated by shining NIR light through the vaginal canal. Thus, the light will have to travel through the vaginal wall to get to the LCE-CB sling. A study that examined both premenopausal and postmenopausal women reported that the average anterior and posterior vaginal wall thickness is between 2.07mm and 2.72mm [78]. Light penetration depth through tissue is largely dependent on the wavelength of the incident light, rather than the intensity of the light [79]. Madsen et al. reported that the penetration depth of 630nm light in pre-and-postmenopausal uteri is 4.79

Author Manuscript Author Manuscript Author Manuscript Author Manuscript

± 0.32mm and 2.59 ± 0.26mm respectively [80]. It has also been reported that the depth of light penetration in the uterus was 2.4 ± 0.22mm and 3.31 ± 0.02mm with 675nm and 835nm light respectively [81]. As such, light wavelength will be an important consideration in ensuring light delivery to the device.

The shape change and temperature increase of the LCE-CB samples were measured in a scar-tissue-like environment. Sling implantation is commonly accompanied by scar tissue formation because of the body's response to foreign materials. A dynamic sling that is expected to modulate its tension reversibly must be able to do so in an environment where stiff tissue surrounds the sling. To simulate such an environment, LCE-CB slings were embedded in agar gels with a modulus of 50kPa (0.5% agar concentration), 100kPa (1% agar concentration), and 150kPa (1.25% Agar concentration) [82]. These experiments demonstrate the LCE-CB sling could change shape in all the agar gels while maintaining the temperature of the agar in the near vicinity, representing surrounding tissue in the physiological setting at a safe range, indicating that these devices can change shape repeatedly in a scar tissue-like environment.

Our results clearly show that the LCE-CB sample can achieve repeatable actuation and temperature response over multiple cycles in simulated physiological conditions. Additionally, the actuation response of the slings can be initiated within the first 30 seconds of IR illumination, showing fast response times. These results are relevant as artificial muscles and sphincters must show repeatable actuation over many cycles with response times relevant to voiding. This response time is dictated by the absorption and thermal properties of the LCE. This stands in contrast to some other biocompatible soft actuators, such as hydrogels, where relatively slow mass transport is typically required for shape change [35].

Finally, we assessed the ability of a device made with LCE-CB material to dynamically alter leakage as controlled by IR illumination when used with a simple *in vitro* urinary tract model. We designed a urinary tract model of stress urinary incontinence by considering the physiology of bladder storage and micturition phases. Micturition control is a complex process involving coordination between multiple urinary tract components, afferent and efferent neural pathways, and multiple neurotransmitters [67,83]. The *in vitro* urethral model developed in this study mimics normal urinary tract on some levels but is limited in that it lacks complex control over the micturition process. In terms of anatomical features, the model bladder cannot contract; however, the backpressure generated due to stored liquid in the bladder initiates urine flow due to gravitational forces. The model urethra has two parts: a soft tube and a stiff plug. Studies have shown that peri-luminal structures in the urethra like the longitudinal smooth muscles, submucous plexus, submucosa, and epithelium act as the central filler volume of the urethra. Relaxed longitudinal smooth muscles during the storage phase cause this urethral central volume to act like a plug that seals off the urethral lumen, while the constricted urethral smooth muscles unseal the urethral lumen [84,85]. In our model, the urethral plug on the inside of the soft urethral tube is intended to function as the central filler volume in the urethra. To simulate the relaxation of the central filler volume which opens the urethral lumen, the outer urethral tube in our model is designed to be much softer and easily extendable. Thus, during the filling of the model bladder, flow

Author Manuscript Author Manuscript Author Manuscript Author Manuscript

through the model urethral increases with increased back pressure as the soft tube stretches open, simulating the increase in intra-abdominal pressure that happens during coughing or sneezing.

Although current static devices to treat SUI are slings, to facilitate the *in vitro* experiment, the LCE-CB was tested as a cuff sutured around the model urethra. The cuff reduced flow through the model urethra by preventing the softer urethral tube to stretch open with increased bladder pressure. The ability of the LCE-CB cuff to establish flow through the model urethra was then studied by shining IR light on it. Our results clearly show that the *in vitro* model could void 20mL of volume significantly faster with IR illumination than no IR illumination. This cuff could operate consistently over multiple cycles of voiding. These results serve as a proof of concept for the ability of the LCE-CB cuff to cause continence then to allow for controlled voiding with IR light illumination. Finally, the LCE-CB cuff was tested *in vivo* in mature, multiparous rabbits, a viable animal model for SUI [86]. LPF testing was performed to ascertain the capability of the LCE-CB cuff to increase LPF and allow for unimpeded voiding on IR illumination. During LPF testing, we observed a significant increase in the average normalized LPF after an LCE-CB cuff was wrapped around the rabbit bladder neck and closed using a suture. This indicated that the cuff was able to increase urethral resistance to leakage. Average normalized LPF during IR illumination was significantly reduced compared to that after cuff implantation. This indicated that IR illumination allows the cuff to lengthen, reducing urethral resistance to urine flow. Finally, normalized LPF during repeat measurements of post implantation in the Implant + IR OFF group was similar to initial post implantation values in the Implant group, indicating that the device could return to its original shape after the light was removed. While increased normalized LPF with cuff implantation and decreased normalized LPF with IR illumination were consistent across all animals, we noticed that one animal had noticeably higher LPF values than the first two (Fig. S5). The higher LPF values in the animal were attributed to increased fibrotic tissue around the rabbit bladder neck. Our results indicate that LCEs are non-cytotoxic; LCEs synthesized with similar chemistries have also been shown to be noncytotoxic [46]. However, we note that long term stability of polythioethers can be compromised in oxidative conditions, which can lead to changes in material properties [87]. Future efforts will involve evaluating changes in the tissue and long-term inflammatory issues due to periodic heating and deformation of the device, as well as chronic IR light delivery. A recently published study, where an actuating device is used for long-term delivery of macromolecular drugs, show that intermittent actuation of the device leads to an improved long-term macromolecule delivery. In this study, the investigators show that intermittent cyclical actuation of an implant could act as an oscillating shield against foreign body response and create a local immunomodulatory effect eliciting temporal changes in capsule formation [88]. Chronic implantation in an animal model is needed, where scar tissue formation around a dynamic device as well as device actuation in scar tissue can be more closely studied. These efforts must also quantify changes in the device in the presence of oxidative environments over a long period of time. Nonetheless, these results serve as a proof of concept for the ability of the shape changing device in the treatment of SUI. One of the main limitations of artificial muscles based on polymeric materials is their low thermal conductivity, leading to a tradeoff

Author Manuscript Author Manuscript Author Manuscript Author Manuscript

between the activation speed and size. To overcome this limitation, future efforts will involve development and study of materials with better heat dissipation ability. Cai et. al. has developed LCE actuators via electrospinning which produces microstructures that are more efficient at heat dissipation and can achieve higher strain rates [89]. Incorporation of Azobenzene dyes with a short half time of the cis state such as those used by Parmeggiani et. al. produces a short-lasting and fast photoinduced thermal effect, allowing for light driven actuations with sub-millisecond dynamics [90].

4. Conclusion

We show that LCE-CB material is capable of shape change in response to IR light and can be used for designing a dynamic device for the treatment of SUI. An LCE-CB device could achieve an actuation strain of 6% even when embedded in a scar-tissue-like environment without exceeding physiologically safe temperatures. We also show that when used as an artificial sphincter type device around an *in vitro* urethral model, the LCE-CB cuff can reduce urine flow through the model urethra. When IR light is illuminated, flow through the model urethra increases. Finally, this device was evaluated *in vivo* in a multiparous rabbit model. Our study showed that the LCE-CB device could increase urethral resistance to leakage under applied abdominal pressure and thus treat conditions such as SUI while modulating such resistance with IR illumination, leading to reduced urethral resistance and improved voiding.

Supplementary Material

Refer to Web version on PubMed Central for supplementary material.

Acknowledgements:

This work was supported by the National Institute of Biomedical Imaging and Bioengineering of the National Institutes of Health under Award Number R21EB028547. The content is solely the responsibility of the authors and does not necessarily represent the official views of the National Institutes of Health. Schematics were created with Biorender (https://biorender.com/).

References

[1]. Lukacz ES, Santiago-Lastra Y, Albo ME, Brubaker L, Urinary Incontinence in Women: A Review, Jama. 318(2017) 1592–1604. 10.1001/jama.2017.12137. [PubMed: 29067433]

[2]. Subak LL, Brown JS, Kraus SR, Brubaker L, Lin F, Richter HE, Bradley CS, Grady D, D.A. of I.S. Group, The “Costs” of Urinary Incontinence for Women, Obstetrics Gynecol. 107 (2006) 908–916. 10.1097/01.aog.0000206213.48334.09.

[3]. Chong EC, Khan AA, Anger JT, The Financial Burden of Stress Urinary Incontinence Among Women in the United States, Curr Urol Rep. 12 (2011) 358. 10.1007/s11934-011-0209-x. [PubMed: 21847532]

[4]. ASHTON-MILLER JA, DeLANCEY JOL, Functional Anatomy of the Female Pelvic Floor, Ann Ny Acad Sci. 1101 (2007) 266–296. 10.1196/annals.1389.034. [PubMed: 17416924]

[5]. DeLancey JOL, Structural support of the urethra as it relates to stress urinary incontinence: The hammock hypothesis, Am J Obstet Gynecol. 170 (1994) 1713–1723. 10.1016/s0002-9378(94)70346-9. [PubMed: 8203431]

[6]. Kalejaiye O, Vij M, Drake MJ, Classification of stress urinary incontinence, World J Urol. 33 (2015) 1215–1220. 10.1007/s00345-015-1617-1. [PubMed: 26108731]

Author Manuscript Author Manuscript Author Manuscript Author Manuscript

[7]. Li J-R, Lei L, Luo N, Chen N, Xu H-T, Hu X, Song Y, Wu Y, Architecture of female urethral supporting structures based on undeformed high-resolution sectional anatomical images, Anat Sci Int. 96 (2021) 30–41. 10.1007/s12565-020-00554-y. [PubMed: 32535854]

[8]. Urinary incontinence in women, Nat Rev Dis Primers. 3 (2017) 17043. 10.1038/nrdp.2017.43.

[9]. DeLancey JOL, Fascial and muscular abnormalities in women with urethral hypermobility and anterior vaginal wall prolapse, Am J Obstet Gynecol. 187 (2002) 93–98. 10.1067/mob.2002.125733. [PubMed: 12114894]

[10]. Haab F, Zimmern PE, Leach GE, Female Stress Urinary Incontinence Due to Intrinsic Sphincteric Deficiency: Recognition and Management, J Urology. 156 (1996) 3–17. 10.1016/s0022-5347(01)65925-1.

[11]. DeLancey JOL, Why do women have stress urinary incontinence?, Neurourol Urodynam. 29 (2010) S13–S17. 10.1002/nau.20888.

[12]. Subak LL, Quesenberry CP, Posner SF, Cattolica E, Soghikian K, The Effect of Behavioral Therapy on Urinary Incontinence, Obstetrics Gynecol. 100 (2002) 72–78. 10.1097/00006250-200207000-00012.

[13]. Moghaddas F, Lidfeldt J, Nerbrand C, Jernström H, Samsioe G, Prevalence of urinary incontinence in relation to self-reported depression, intake of serotonergic antidepressants, and hormone therapy in middle-aged women: a report from the Women's Health in the Lund Area study, Menopause. 12 (2005) 318–324. 10.1097/01.gme.0000143736.17715.55. [PubMed: 15879921]

[14]. Jahromi MK, Talebizadeh M, Mirzaei M, The Effect of Pelvic Muscle Exercises on Urinary Incontinency and Self-Esteem of Elderly Females With Stress Urinary Incontinency, 2013, Global J Heal Sci. 7 (2015) 71–79. 10.5539/gjhs.v7n2p71.

[15]. Ghoniem G, Corcos J, Comiter C, Westney OL, Herschorn S, Durability of Urethral Bulking Agent Injection for Female Stress Urinary Incontinence: 2-Year Multicenter Study Results, J Urology. 183 (2010) 1444–1449. 10.1016/j.juro.2009.12.038.

[16]. Cox A, Herschorn S, Lee L, Surgical management of female SUI: is there a gold standard?, Nat Rev Urol. 10 (2013) 78–89. 10.1038/nrurol.2012.243. [PubMed: 23318365]

[17]. Bandukwala NQ, Gousse AE, Mixed Urinary Incontinence: What First?, Curr Urol Rep. 16 (2015) 9. 10.1007/s11934-015-0483-0. [PubMed: 25677232]

[18]. Wu Y. (Maria), Welk B, Revisiting current treatment options for stress urinary incontinence and pelvic organ prolapse: a contemporary literature review, Res Reports Urology. 11 (2019) 179–188. 10.2147/rru.s191555.

[19]. Lo T-S, Shailaja N, Tan YL, Wu M-P, Chua S, Roy KW, Outcomes and failure risks in mid-urethral sling insertion in elderly and old age with urodynamic stress incontinence, Int Urogynecol J. 31 (2020) 717–726. 10.1007/S00192-019-04171-w. [PubMed: 31832716]

[20]. LENG WW, DAVIES BJ, TARIN T, SWEENEY DD, CHANCELLOR MB, DELAYED TREATMENT OF BLADDER OUTLET OBSTRUCTION AFTER SLING SURGERY, J Urology. 172 (2004) 1379–1381. 10.1097/01.ju.0000138555.70421.ca.

[21]. Lee D, Zimmern PE, Management of complications of mesh surgery, Curr Opin Urol. 25 (2015) 284–291. 10.1097/mou.0000000000000187. [PubMed: 26049869]

[22]. Rackley RR, Abdelmalak JB, Tchetgen MB, Madjar S, Jones S, Noble M, Tension-free vaginal tape and percutaneous vaginal tape sling procedures., Techniques Urology. 7 (2001) 90–100.

[23]. Daneshgari F, Kong W, Swartz M, Complications of Mid Urethral Slings: Important Outcomes for Future Clinical Trials, J Urology. 180 (2008) 1890–1897. 10.1016/j.juro.2008.07.029.

[24]. Rich SI, Wood RJ, Majidi C, Untethered soft robotics, Nat Electron. 1 (2018) 102–112. 10.1038/s41928-018-0024-1.

[25]. Zhang X, Chen L, Lim KH, Gonuguntla S, Lim KW, Pranantyo D, Yong WP, Yam WJT, Low Z, Teo WJ, Nien HP, Loh QW, Soh S, The Pathway to Intelligence: Using Stimuli-Responsive Materials as Building Blocks for Constructing Smart and Functional Systems, Adv Mater. 31 (2019) 1804540. 10.1002/adma.201804540.

[26]. Makaran ohn E., Dittmer DK, Buchal RO, MacArthur DE, The SMART Wrist-Hand Orthosis (WHO) for Quadriplegic Patients, Jpo J Prosthetics Orthot. 5 (1993) 73/27–30/76. 10.1097/00008526-199307000-00002.

Author Manuscript Author Manuscript Author Manuscript Author Manuscript

[27]. Pfeiffer C, DeLaurentis K, Mavroidis C, Shape memory alloy actuated robot prostheses: initial experiments, Proc 1999 leee Int Conf Robotics Automation Cat 99ch36288c. 3 (1999) 2385–2391 vol.3. 10.1109/robot.1999.770462.

[28]. Bundhoo V, Park EJ, Design of an Artificial Muscle Actuated Finger towards Biomimetic Prosthetic Hands, Icar '05 Proc 12th Int Conf Adv Robotics 2005. (2005) 368–375. 10.1109/icar.2005.1507437.

[29]. Icardi U, Large bending actuator made with SMA contractile wires: theory, numerical simulation and experiments, Compos Part B Eng. 32 (2001) 259–267. 10.1016/s1359-8368(00)00062-7.

[30]. Barrett R, Gross RS, Super-active shape-memory alloy composites, Smart Mater Struct. 5 (1996) 255. 10.1088/0964-1726/5/3/003.

[31]. Price A, Edgerton A, Cocaud C, Naguib H, Jnifene A, A Study on the Thermomechanical Properties of Shape Memory Alloys-based Actuators used in Artificial Muscles, J Intel Mat Syst Str. 18 (2007) 11–18. 10.1177/1045389x06064000.

[32]. Fernandes C, Heggannavar GB, Kariduraganavar MY, Mitchell GR, Alves N, Morouço P, Smart Materials for Biomedical Applications: The Usefulness of Shape-Memory Polymers, Appl Mech Mater. 890 (2019) 237–247. 10.4028/www.scientific.net/amm.890.237.

[33]. Liu Z, Calvert P, Multilayer Hydrogels as Muscle-Like Actuators, Adv Mater. 12 (2000) 288–291. 10.1002/(sici)1521-4095(200002)12:4<288::aid-adma288>3.0.co;2-1.

[34]. Keplinger C, Sun J-Y, Foo CC, Rothemund P, Whitesides GM, Suo Z, Stretchable, Transparent, Ionic Conductors, Science. 341 (2013) 984–987. 10.1126/science.1240228. [PubMed: 23990555]

[35]. Mirvakili SM, Hunter IW, Artificial Muscles: Mechanisms, Applications, and Challenges, Adv Mater. 30 (2018) 1704407. 10.1002/adma.201704407.

[36]. White TJ, Broer DJ, Programmable and adaptive mechanics with liquid crystal polymer networks and elastomers, Nat Mater. 14(2015) 1087–1098. 10.1038/nmat4433. [PubMed: 26490216]

[37]. Finkelmann H, Kock H, Rehage G, Investigations on liquid crystalline polysiloxanes 3. Liquid crystalline elastomers — a new type of liquid crystalline material, Die Makromolekulare Chemie Rapid Commun. 2 (1981) 317–322. 10.1002/marc.1981.030020413.

[38]. Kularatne RS, Kim H, Boothby JM, Ware TH, Liquid crystal elastomer actuators: Synthesis, alignment, and applications, J Polym Sci Part B Polym Phys. 55 (2017) 395–411. 10.1002/polb.24287.

[39]. Saed MO, Torbati AH, Starr CA, Visvanathan R, Clark NA, Yakacki CM, Thiol-acrylate main-chain liquid-crystalline elastomers with tunable thermomechanical properties and actuation strain, J Polym Sci Part B Polym Phys. 55 (2017) 157–168. 10.1002/polb.24249.

[40]. Xia Y, Zhang X, Yang S, Instant Locking of Molecular Ordering in Liquid Crystal Elastomers by Oxygen-Mediated Thiol-Acrylate Click Reactions, Angewandte Chemie Int Ed. 57 (2018) 5665–5668. 10.1002/anie.201800366.

[41]. Lu H-F, Wang M, Chen X-M, Lin B-P, Yang H, Interpenetrating Liquid-Crystal Polyurethane/Polyacrylate Elastomer with Ultrastrong Mechanical Property, J Am Chem Soc. 141 (2019) 14364–14369. 10.1021/jacs.9b06757. [PubMed: 31429282]

[42]. Thomsen DL, Keller P, Naciri J, Pink R, Jeon H, Shenoy D, Ratna BR, Liquid Crystal Elastomers with Mechanical Properties of a Muscle, Macromolecules. 34 (2001) 5868–5875. 10.1021/ma001639q.

[43]. Ambulo CP, Tasmim S, Wang S, Abdelrahman MK, Zimmern PE, Ware TH, Processing advances in liquid crystal elastomers provide a path to biomedical applications, J Appl Phys. 128 (2020) 140901. 10.1063/5.0021143. [PubMed: 33060862]

[44]. Saed MO, Ambulo CP, Kim H, De R, Raval V, Searles K, Siddiqui DA, Cue JMO, Stefan MC, Shankar MR, Ware TH, Molecularly-Engineered, 4D-Printed Liquid Crystal Elastomer Actuators, Adv Funct Mater. 29 (2019) 1806412. 10.1002/adfm.201806412.

[45]. Kotikian A, McMahan C, Davidson EC, Muhammad JM, Weeks RD, Daraio C, Lewis JA, Untethered soft robotic matter with passive control of shape morphing and propulsion, Sci Robotics. 4 (2019) eaax7044. 10.1126/scirobotics.aax7044.

[46]. Yakacki CM, Saed M, Nair DP, Gong T, Reed SM, Bowman CN, Tailorable and programmable liquid-crystalline elastomers using a two-stage thiol–acrylate reaction, Rsc Adv. 5 (2015) 18997–19001. 10.1039/c5ra01039j.

Author Manuscript Author Manuscript Author Manuscript Author Manuscript

[47]. Traugutt NA, Volpe RH, Bollinger MS, Saed MO, Torbati AH, Yu K, Dadivanyan N, Yakacki CM, Liquid-crystal order during synthesis affects main-chain liquid-crystal elastomer behavior, Soft Matter. 13 (2017) 7013–7025. 10.1039/c7sm01405h. [PubMed: 28930352]

[48]. Li M-H, Keller P, Artificial muscles based on liquid crystal elastomers, Philosophical Transactions Royal Soc Math Phys Eng Sci. 364 (2006) 2763–2777. 10.1098/rsta.2006.1853.

[49]. Burke KA, Rousseau IA, Mather PT, Reversible actuation in main-chain liquid crystalline elastomers with varying crosslink densities, Polymer. 55 (2014) 5897–5907. 10.1016/j.polymer.2014.06.088.

[50]. Dewhirst MW, Viglianti BL, Lora-Michiels M, Hanson M, Hoopes PJ, Basic principles of thermal dosimetry and thermal thresholds for tissue damage from hyperthermia, Int J Hyperther. 19 (2009) 267–294. 10.1080/0265673031000119006.

[51]. Kim H, Lee JA, Ambulo CP, Lee HB, Kim SH, Naik VV, Haines CS, Aliev AE, Ovalle-Robles R, Baughman RH, Ware TH, Intelligently Actuating Liquid Crystal Elastomer-Carbon Nanotube Composites, Adv Funct Mater. 29 (2019) 1905063. 10.1002/adfm.201905063.

[52]. Zeng H, Wasylczyk P, Wiersma DS, Priimagi A, Light Robots: Bridging the Gap between Microrobotics and Photomechanics in Soft Materials, Adv Mater. 30 (2018) 1703554. 10.1002/adma.201703554.

[53]. Ambulo CP, Ford MJ, Searles K, Majidi C, Ware TH, 4D-Printable Liquid Metal-Liquid Crystal Elastomer Composites, Acs Appl Mater Inter. 13 (2020) 12805–12813. 10.1021/acsami.0c19051.

[54]. Opel DR, Hagstrom E, Pace AK, Sisto K, Hirano-Ali SA, Desai S, Swan J, Light-emitting Diodes: A Brief Review and Clinical Experience., J Clin Aesthetic Dermatology. 8 (2015) 36–44.

[55]. Corona-Quintanilla DL, Castelan F, Fajardo V, Manzo J, Martinez-Gomez M, Temporal Coordination of Pelvic and Perineal Striated Muscle Activity During Micturition in Female Rabbits, J Urology. 181 (2009) 1452–1458. 10.1016/j.juro.2008.10.103.

[56]. Celayir S, Effects of Different Sex Hormones on Male Rabbit Urodynamics: An Experimental Study, Horm Res Paediat. 60 (2003) 215–220. 10.1159/000074034.

[57]. HIJAZ A, DANESHGARI F, CANNON T, DAMASER M, EFFICACY OF A VAGINAL SLING PROCEDURE IN A RAT MODEL OF STRESS URINARY INCONTINENCE, J Urology. 172 (2004) 2065–2068. 10.1097/01.ju.0000138476.42556.b8.

[58]. Dietz HP, Mouritsen L, Ellis G, Wilson PD, Does the tension-free vaginal tape stay where you put it?, Am J Obstet Gynecol. 188 (2003) 950–953. 10.1067/mob.2003.268. [PubMed: 12712092]

[59]. Krambeck AE, Dora CD, Sebo TJ, Rohlinger AL, DiMarco DS, Elliott DS, Time-dependent variations in inflammation and scar formation of six different pubovaginal sling materials in the rabbit model, Urology. 67 (2006) 1105–1110. 10.1016/j.urology.2005.11.036. [PubMed: 16698388]

[60]. Ambulo CP, Burroughs JJ, Boothby JM, Kim H, Shankar MR, Ware TH, Four-dimensional Printing of Liquid Crystal Elastomers, Acs Appl Mater Inter. 9 (2017) 37332–37339. 10.1021/acsami.7b11851.

[61]. Ceamanos L, Kahveci Z, Lopez-Valdeolivas M, Liu D, Broer DJ, Sanchez-Somolinos C, Four-Dimensional Printed Liquid Crystalline Elastomer Actuators with Fast Photoinduced Mechanical Response toward Light-Driven Robotic Functions, Acs Appl Mater Inter. 12 (2020) 44195–44204. 10.1021/acsami.0c13341.

[62]. Kotikian A, Truby RL, Boley JW, White TJ, Lewis JA, 3D Printing of Liquid Crystal Elastomeric Actuators with Spatially Programed Nematic Order, Adv Mater. 30 (2018) 1706164. 10.1002/adma.201706164.

[63]. Ren L, Li B, He Y, Song Z, Zhou X, Liu Q, Ren L, Programming Shape-Morphing Behavior of Liquid Crystal Elastomers via Parameter-Encoded 4D Printing, Acs Appl Mater Inter. 12 (2020) 15562–15572. 10.1021/acsami.0c00027.

[64]. Nayar VT, Weiland JD, Nelson CS, Hodge AM, Elastic and viscoelastic characterization of agar, J Mech Behav Biomed. 7 (2012) 60–68. 10.1016/j.jmbbm.2011.05.027.

[65]. Moksnes LR, Svenningsen R, Schiøtz HA, Moe K, Staff AC, Kulseng-Hanssen S, Sling mobilization in the management of urinary retention after mid-urethral sling surgery, Neurourol Urodynam. 36 (2017) 1091—1096. 10.1002/nau.23046.

Author Manuscript Author Manuscript Author Manuscript Author Manuscript

[66]. Pham KN, Topp N, Guralnick ML, Koduri S, Newcomer JR, O'Connor RC, Preoperative Valsalva voiding increases the risk of urinary retention after midurethral sling placement, Int Urogynecol J. 21 (2010) 1243–1246. 10.1007/s00192-010-1177-2. [PubMed: 20480139]

[67]. Wolff BJ, Hart S, Joyce CJ, Eubanks RB, Mueller ER, Pham TT, Urinary retention is rare after colpocleisis and concomitant midurethral sling: a 10-year experience, Int Urogynecol J. 32 (2021) 729–736. 10.1007/S00192-021-04705-1. [PubMed: 33547907]

[68]. Darrah DM, Griebling TL, Silverstein JH, Postoperative Urinary Retention, Anesthesiol Clin. 27 (2009) 465–484. 10.1016/j.anclin.2009.07.010. [PubMed: 19825487]

[69]. Kim JH, Shin SH, Oh MM, Park JY, Lee JG, Bae JH, Factors affecting transient urinary retention after transobturator tape mid-urethral sling surgery for female patients with stress urinary incontinence: a single center experience, Eur J Obstet Gyn R B. 168 (2013) 107–111. 10.1016/j.ejogrb.2012.12.013.

[70]. HAN J, LEE K, CHOO M, Management of Recurrent or Persistent Stress Urinary Incontinence after Midurethral Sling, Luts Low Urin Tract Symptoms. 4 (2012) 95–101. 10.1111/j.1757-5672.2011.00129.x. [PubMed: 26676707]

[71]. Moritz A. Re, and F CH Jr., Studies of thermal injury: II. The relative importance of time and surface temperature in the causation of cutaneous burns, The American Journal of Pathology. 23 (1947) 695. [PubMed: 19970955]

[72]. Ong BB, Encyclopedia of Forensic and Legal Medicine, Article Titles (2005) 90–98. 10.1016/b0-12-369399-3/00209-3.

[73]. Stoll AM, Greene LC, Relationship between pain and tissue damage due to thermal radiation, J Appl Physiol. 14 (1959) 373–382. 10.1152/jappl.1959.14.3.373. [PubMed: 13654166]

[74]. Roizin-Towle L, Pirro JP, The response of human and rodent cells to hyperthermia, Int J Radiat Oncol Biology Phys. 20 (1991) 751–756. 10.1016/0360-3016(91)90018-y.

[75]. Maytin EV, Wimberly JM, Anderson RR, Thermotolerance and the Heat Shock Response in Normal Human Keratinocytes in Culture, J Invest Dermatol. 95 (1990) 635–642. 10.1111/1523-1747.ep12514303. [PubMed: 2250106]

[76]. Law MP, Coultas PG, Field SB, Induced thermal resistance in the mouse ear, Br J Radiology. 52 (1979) 308–314. 10.1259/0007-1285-52-616-308.

[77]. Maytin EV, Wmberly JM, Kane KS, Heat Shock Modulates UVB-Induced Cell Death in Human Epidermal Keratinocytes: Evidence for a Hyperthermia-Inducible Protective Response, J Invest Dermatol. 103 (1994) 547–553. 10.1111/1523-1747.ep12396274. [PubMed: 7930680]

[78]. Lara LADS, Silva ARD, Rosa-e-Silva JC, Chaud F, Silva-de-Sá MF, e Silva ARM, Rosa-e-Silva ACJDS, Menopause Leading to Increased Vaginal Wall Thickness in Women with Genital Prolapse: Impact on Sexual Response, J Sex Medicine. 6 (2009) 3097–3110. 10.1111/j.1743-6109.2009.01407.x.

[79]. Lanzafame RJ, de la Torre S, Leibaschoff GH, The Rationale for Photobiomodulation Therapy of Vaginal Tissue for Treatment of Genitourinary Syndrome of Menopause: An Analysis of Its Mechanism of Action, and Current Clinical Outcomes, Photobiomodulation Photomed Laser Surg. 37 (2019) 395–407. 10.1089/photob.2019.4618.

[80]. Madsen SJ, Wyss P, Svaasand LO, Haskell RC, Tadir Y, Tromberg BJ, Determination of the optical properties of the human uterus using frequency-domain photon migration and steady-state techniques, Phys Medicine Biology. 39 (1994) 1191–1202. 10.1088/0031-9155/39/8/001.

[81]. Stolik S, Delgado JA, Pérez A, Anasagasti L, Measurement of the penetration depths of red and near infrared light in human "ex vivo" tissues, J Photochem Photobiology B Biology. 57 (2000) 90–93. 10.1016/s1011-1344(00)00082-8.

[82]. Nayar VT, Weiland JD, Nelson CS, Hodge AM, Elastic and viscoelastic characterization of agar, J Mech Behav Biomed. 7 (2012) 60–68. 10.1016/j.jmbbm.2011.05.027.

[83]. Park BH, Kim JC, Kim HW, Kim YH, Choi JB, Lee DH, Midterm Efficacy and Complications of Readjustable Midurethral Sling (Remeex System) in Female Stress Urinary Incontinence Wth Recurrence or Intrinsic Sphincter Deficiency, Urology. 85 (2015) 79–84. 10.1016/j.urology.2014.10.003. [PubMed: 25530367]

Author Manuscript Author Manuscript Author Manuscript Author Manuscript

[84]. Mistry MA, Klarskov N, DeLancey JO, Lose G, A structured review on the female urethral anatomy and innervation with an emphasis on the role of the urethral longitudinal smooth muscle, Int Urogynecol J. 31 (2020) 63–71. 10.1007/s00192-019-04104-7. [PubMed: 31529330]

[85]. Schäfer W, Some Biomechanical Aspects of Continence Function, Scand J Urol Nephrol. 35 (2001) 44–60. 10.1080/003655901750174890. [PubMed: 11291687]

[86]. Hernandez-Reynoso AG, Corona-Guintanilla DL, López-García K, Horbovetz AA, Castelán F, Zimmern P, Martínez-Gómez M, Romero-Ortega M.l., Targeted neuromodulation of pelvic floor nerves in aging and multiparous rabbits improves continence, Sci Rep-Uk. 11 (2021) 10615. 10.1038/s41598-021-90088-8.

[87]. Javed M, Tasmim S, Abdelrahman MK, Ambulo CP, Ware TH, Degradation-Induced Actuation in Oxidation-Responsive Liquid Crystal Elastomers, Crystals. 10 (2020) 420. 10.3390/cryst10050420. [PubMed: 33936789]

[88]. Whyte W, Goswami D, Wang SX, Fan Y, Ward NA, Levey RE, Beatty R, Robinson ST, Sheppard D, O'Connor R, Monahan DS, Trask L, Mendez KL, Varela CE, Horvath MA, Wylie R, O'Dwyer J, Domingo-Lopez DA, Rothman AS, Duffy GP, Dolan EB, Roche ET, Dynamic actuation enhances transport and extends therapeutic lifespan in an implantable drug delivery platform, Nat Commun. 13 (2022) 4496. 10.1038/s41467-022-32147-w. [PubMed: 35922421]

[89]. He O, Wang Z, Wang Y, Wang Z, Li C, Annapooranan R, Zeng J, Chen R, Cai S, Electrospun liquid crystal elastomer microfiber actuator, Sci Robotics. 6 (2021). 10.1126/scirobotics.abi9704.

[90]. Ferrantini C, Pioner JM, Martella D, Coppini R, Piroddi N, Paoli P, Calamai M, Pavone FS, Wiersma DS, Tesi C, Cerbai E, Poggesi C, Sacconi L, Parmeggiani C, Development of Light-Responsive Liquid Crystalline Elastomers to Assist Cardiac Contraction, Circ Res. 124 (2019) e44–e54. 10.1161/circresaha.118.313889. [PubMed: 30732554]

Author Manuscript Author Manuscript Author Manuscript Author Manuscript

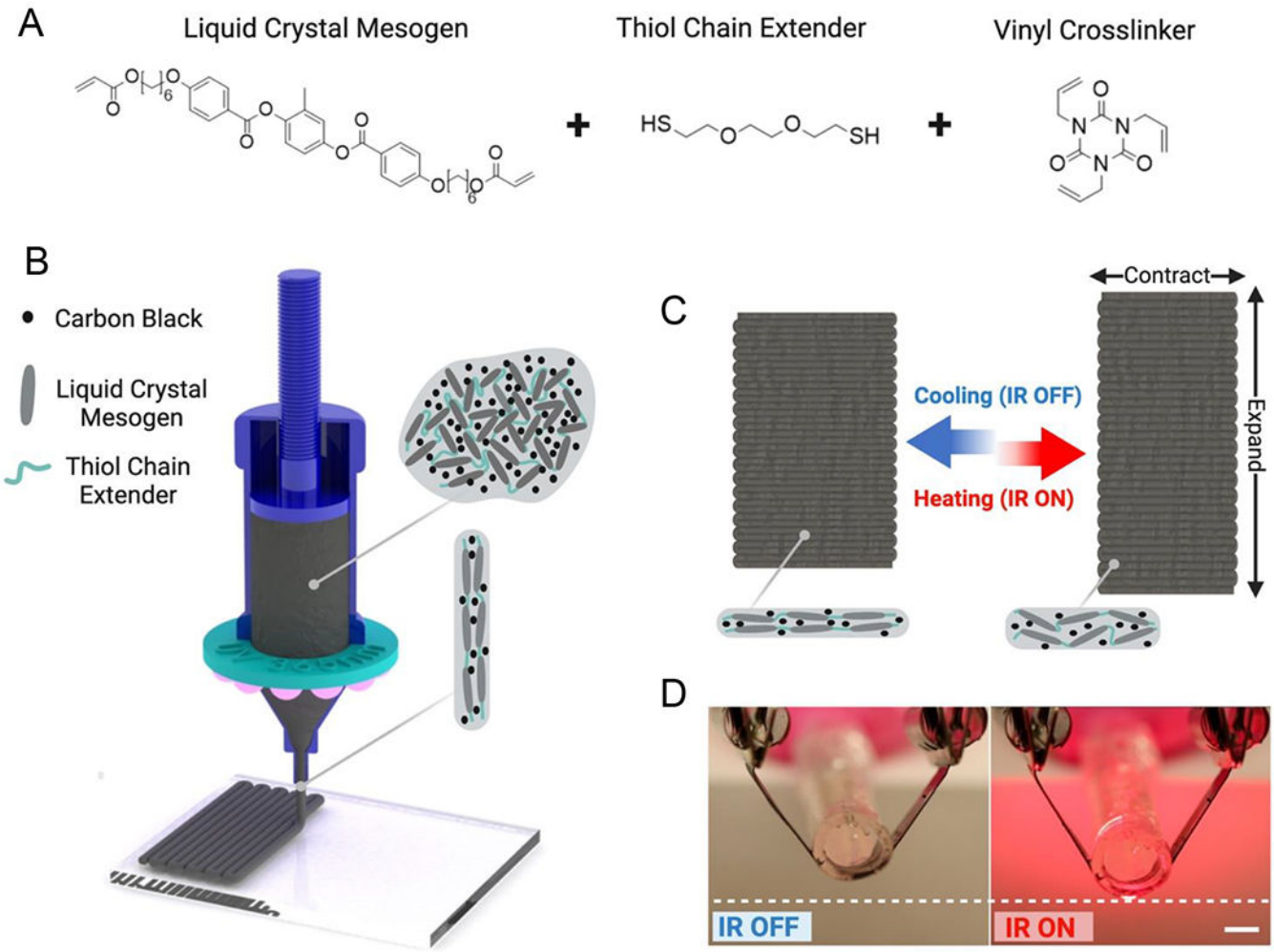

Figure 1.

LCE-CB sling fabrication and actuation mechanism. A) Monomers used for synthesizing LC ink with embedded CB particles. B) Schematic of 3D printing fabrication of LCE-CB slings. C) Schematic of shape-morphing stimulus response of 3D printed LCE-CB slings. D) Photothermal actuation of 3D printed LCE-CB composite with IR light in the open air, scale bar: 5mm.

Author Manuscript Author Manuscript Author Manuscript Author Manuscript

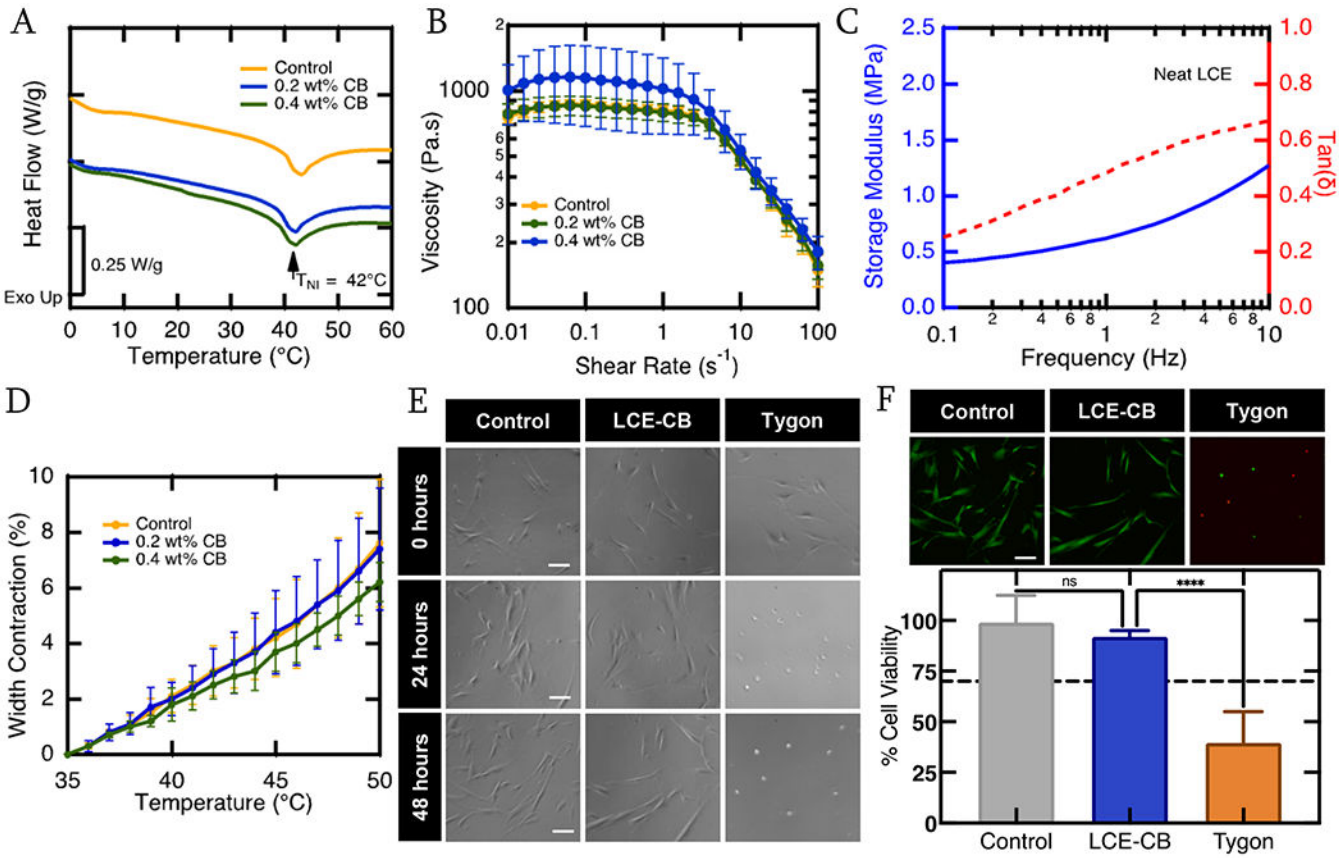

Figure 2.

Material Characterization. A) Representative DSC curves showing heat flow of LC ink without CB particles (yellow), 0.2 wt% CB concentration (Blue), and 0.4 wt% CB concentration (green) as a function of temperature. All three compositions exhibit an endothermic peak representing actuation (transition) temperature. B) Log-log plots of viscosity of the LC ink with 0 wt% – 0.4 wt% CB concentration as a function of shear rate at 38°C. C). Representative DMA curve showing storage modulus (solid blue) and tan delta (dashed red) as a function of frequency of a polydomain neat LCE sample. D) Heat actuation curve of rectangular 3D printed LCE samples with 0 wt% - 0.4 wt% CB concentration and uniaxial alignment along the short axis of the rectangle. Three samples are evaluated from three different batches for each composition (n=9). Error bars represent standard deviation. (E) Phase contrast micrographs of hDFAs at 0, 24, and 48 hours in the control, LCE extract and tygon extract media. Scale bars = 100 μm. (F) Representative fluorescent micrographs of the Live(green)/Dead(red) assay for hDFAs after 48 hours in control, LCE-CB extract or Tygon extract media. Scale bars = 100 μm. Quantification of live cell percentage for control, LCE-CB extract and tygon extract media conditions after 48 hours. Results shown are mean with standard error of mean. Statistical significance is noted as: ****p<0.0001, one way ANOVA. (n=3).

Author Manuscript Author Manuscript Author Manuscript Author Manuscript

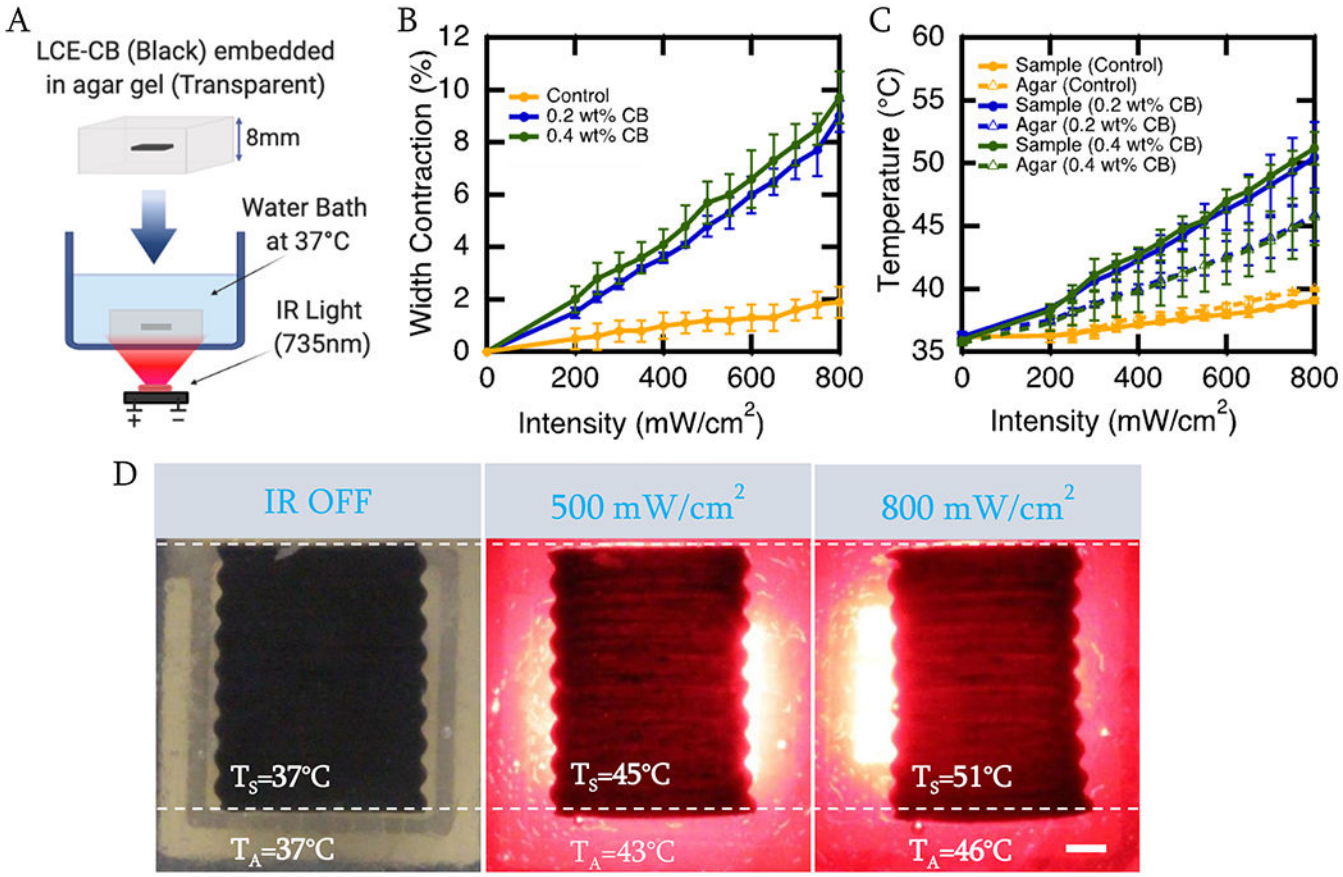

Figure 3.

Shape Change of LCE-CB sample with varying CB concentrations in response to varying IR light intensities. A) Schematic showing the setup used to analyze the shape change and temperature response of the LCE-CB sample in response to IR light. B) Photothermal actuation curve of neat LCE and LCE-CB sample with varying CB concentrations embedded in 0.5% agar in response to varying IR light intensities. C) Temperature measurement of neat LCE and LCE-CB samples with varying CB concentrations embedded in 0.5% agar in response to varying IR light intensities. Temperatures are measured at the sample surface and agar surrounding the sample (2mm vicinity) after 2 minutes of continuous IR light irradiation. D) Images showing contraction along the width and elongation along the length, as well as temperature of the sample (TS) and surrounding agar (TA) of an LCE-CB sample with 0.4 wt% CB embedded in 0.5% agar gel. LCE-CB sample at 0 seconds with IR off (left), sample actuation and temperature measured after irradiation with 500 mW/cm^2 IR light for 120 seconds (middle), and sample actuation and temperature measured after irradiation with 800 mW/cm^2 IR light for 120 seconds (right). Three samples are evaluated from three different batches for each composition (n=9 for each composition). Error bars represent standard deviation. Scale bar: 1mm.

Author Manuscript Author Manuscript Author Manuscript Author Manuscript

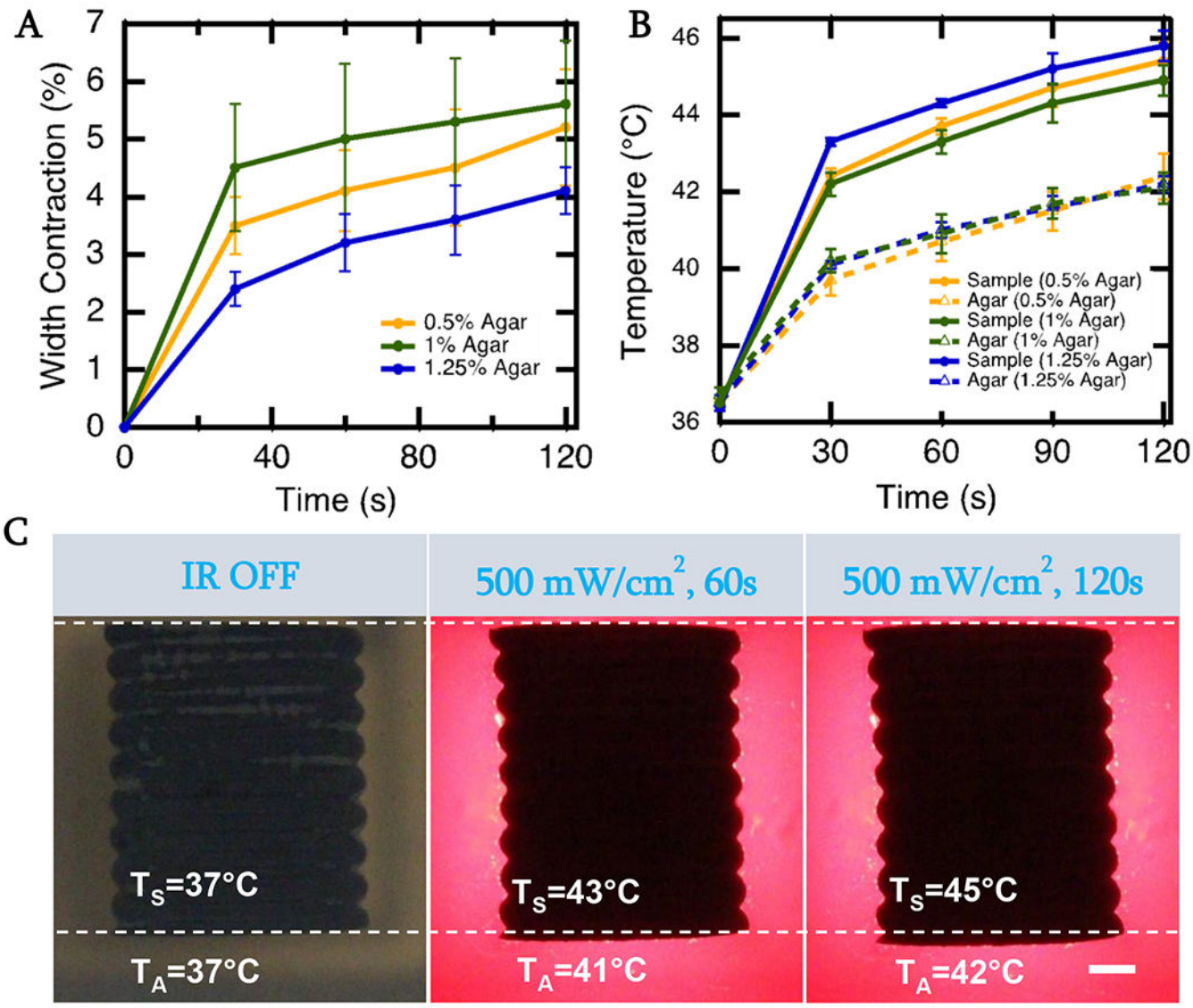

Figure 4.

Shape Change of LCE-CB sample in scar-tissue-like environment A) Photothermal actuation curves of LCE-CB sample with 0.4 wt% CB embedded in agar gels with varying agar concentration measured over 2 minutes of continuous 500mW/cm^2 IR light irradiation. C) Temperature measurement of LCE-CB sample embedded in agar gels with varying agar concentration measured after 2 minutes of continuous 500mW/cm^2 IR light irradiation. Temperatures are measured at the sample surface (TS) and agar surrounding the sling (TA) (2mm vicinity) after 2 minutes of continuous IR light irradiation. D) Images showing contraction along the width and elongation along the length and temperature of the sample and surrounding agar of an LCE-CB sling with 0.4 wt% CB embedded in 1% agar gel. LCE-CB sample at 0 seconds with IR off (left), sample actuation and temperature measured after irradiation with 500 mW/cm^2 IR light for 60 seconds (middle), and sample actuation and temperature measured after irradiation with 500 mW/cm^2 IR light for 120 seconds.

Author Manuscript Author Manuscript Author Manuscript Author Manuscript

Three samples are evaluated from three different batches in each agar gel (n=9 for each composition). Error bars represent standard deviation. Scale bar: 1mm.

Author Manuscript
Author Manuscript
Author Manuscript
Author Manuscript

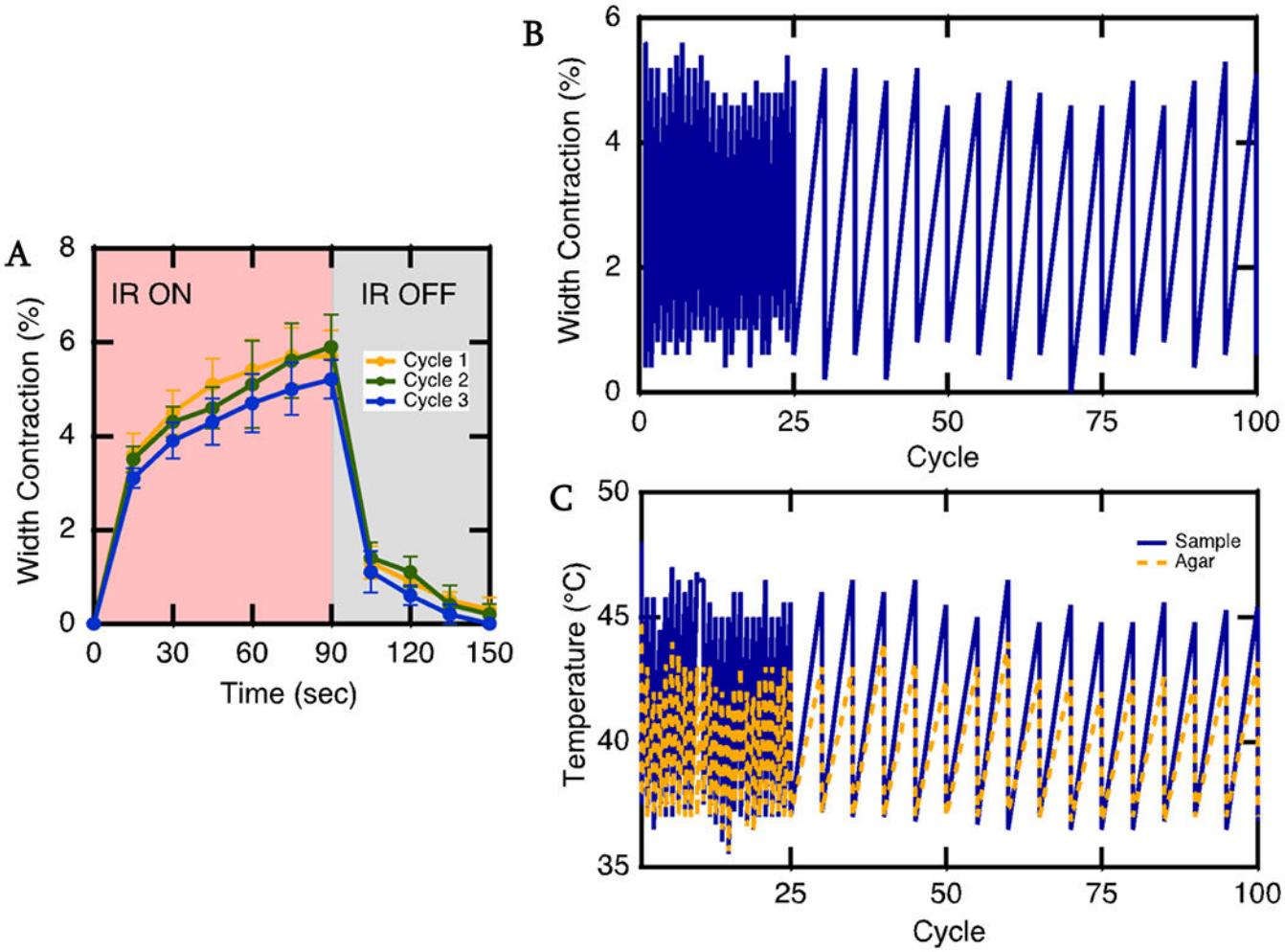

Figure 5.

Actuation curve and cyclic actuation of LCE-CB sample. A) Actuation onset and offset of an LCE-CB sample with 0.4 wt% CB concentration embedded in 1% agar Illuminated with 500 mW/cm^2 intensity IR light. IR light is on for 90 seconds, then off for 60 seconds B) Cyclic Actuation of LCE-CB sample with 0.4 wt% CB embedded in 1% agar gel. C) Corresponding temperature of the device (blue solid line) and surrounding agar (yellow dashed line) during the cyclic actuation test. Embedded samples are irradiated with 500 mW/cm^2 IR light for 2 mins, then allowed to return to the original shape over 60 seconds. This test is repeated over 100 cycles. (n=1). Error bars represent standard deviation.

Author Manuscript Author Manuscript Author Manuscript Author Manuscript

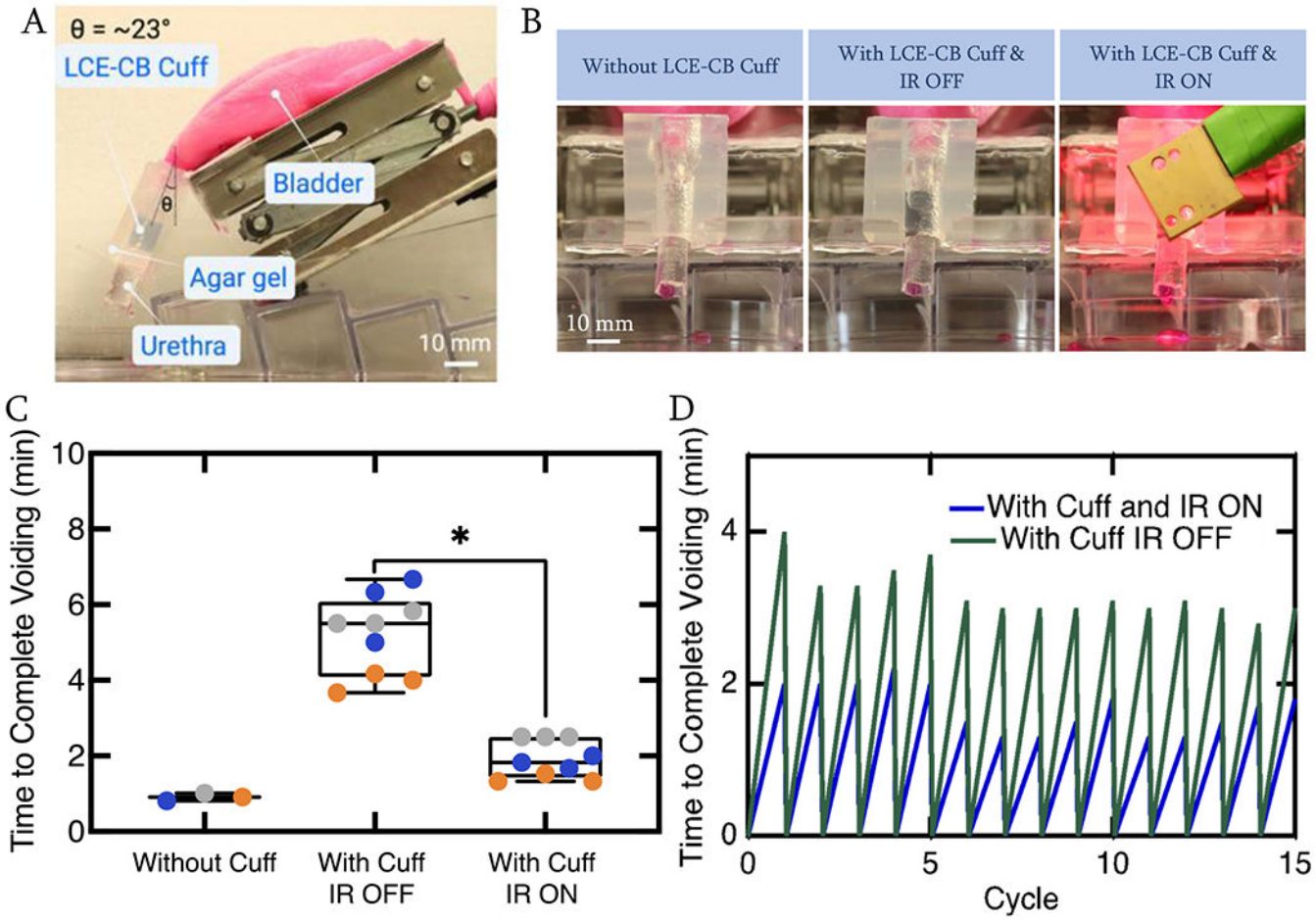

Figure 6.

Actuation of LCE-CB cuff in an in vitro urinary tract model. A) Image showing the in vitro urinary model B) Images showing snapshots of a model urethra with no LCE-CB cuff around (left), with LCE-CB cuff around the urethra and IR light off (Middle), and with LCE-CB cuff around the urethra and IR light on condition (right). A slab of 1% agar gel cut in the negative shape of the model urethra is placed on top of the urethra to mimic tissue surrounding the urethra. C) Duration of time necessary for the model urethra to void 19mL of water with no LCE-CB cuff, with LCE-CB cuff and IR light off, and with LCE-CB cuff and IR light on conditions. Three different LCE-CB cuffs were tested over three voiding cycles. Data from each cycle is represented in a different color. A p-value less than 0.05 was considered statistically significant. D) One LCE-CB cuff is tested over 15 cycles of voiding in the IR light off and IR light on conditions, and voiding time for 19 mL of water is recorded. (n=1). Error bars represent standard deviation. Statistical significance is noted as: *p=0.0397, one way ANOVA.

Author Manuscript Author Manuscript Author Manuscript Author Manuscript

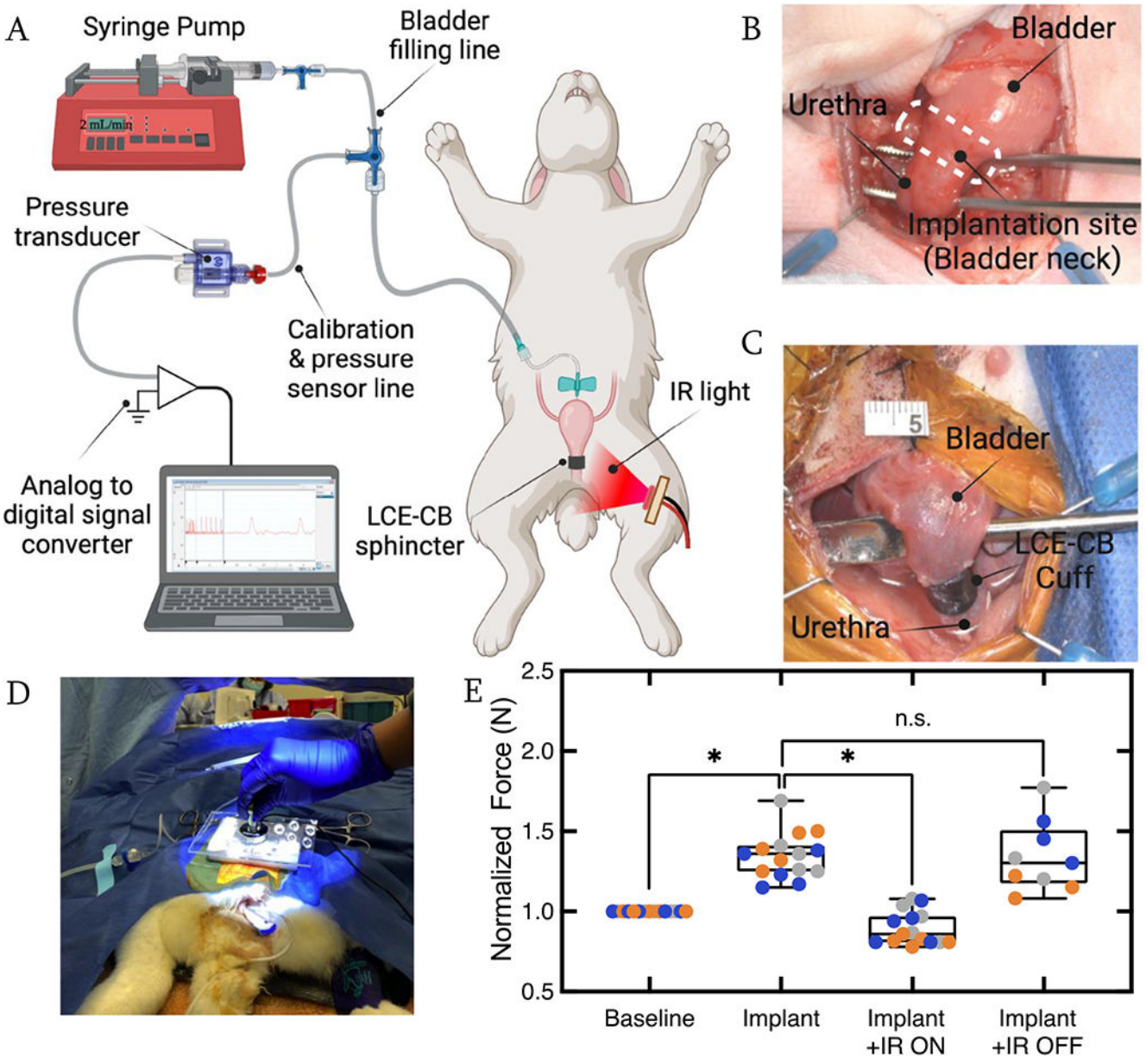

Figure 7.

LCE-CB cuff analysis in multiparous rabbit. A) Schematic illustrating the catheterization of rabbit bladder using a butterfly catheter. B) Image of rabbit bladder and bladder neck exposed. C) Image showing an LCE-CB cuff implanted around the rabbit bladder neck. D) Snapshot of force applied to rabbit abdomen on top of the bladder dome. E) Box plot showing normalized abdominal force required to cause leakage at baseline, after device implantation (Implant), during IR actuation (Implant +IR ON), and redo of the implant with IR off condition (Implant + IR OFF). Data from each experimental replicate is presented in a different color. Statistical significance is noted as: *p=0.0231 (implant vs. implant + IR ON),

*p=0.0138 (baseline vs. implant) paired t test. (n=3 with five repeat measurements for each study group in each animal). Error bars represent standard deviation.

Author Manuscript Author Manuscript Author Manuscript Author Manuscript